



HAL
open science

Active Back-Arc Thrust in North West Java, Indonesia

Sonny Aribowo, Laurent Husson, Danny H. Natawidjaja, Christine Authemayou, Mudrik R. Daryono, Anggraini R. Puji, Pierre G. Valla, Astyka Pamumpuni, Dadan D. Wardhana, Gino de Gelder, et al.

► **To cite this version:**

Sonny Aribowo, Laurent Husson, Danny H. Natawidjaja, Christine Authemayou, Mudrik R. Daryono, et al.. Active Back-Arc Thrust in North West Java, Indonesia. *Tectonics*, 2022, 41, 10.1029/2021TC007120 . insu-03779799

HAL Id: insu-03779799

<https://insu.hal.science/insu-03779799>

Submitted on 18 Sep 2022

HAL is a multi-disciplinary open access archive for the deposit and dissemination of scientific research documents, whether they are published or not. The documents may come from teaching and research institutions in France or abroad, or from public or private research centers.

L'archive ouverte pluridisciplinaire **HAL**, est destinée au dépôt et à la diffusion de documents scientifiques de niveau recherche, publiés ou non, émanant des établissements d'enseignement et de recherche français ou étrangers, des laboratoires publics ou privés.



Distributed under a Creative Commons Attribution - NonCommercial 4.0 International License

Key Points:

- Major active, seismogenic back-arc thrust in northwest Java
- The fault initiated during Pliocene and propagates westwards
- Intricate relationships between fault propagation, volcanic activity and foreland sedimentation

Correspondence to:

S. Aribowo,
sonny.aribowo@univ-grenoble-alpes.fr

Citation:

Aribowo, S., Husson, L., Natawidjaja, D. H., Authemayou, C., Daryono, M. R., Puji, A. R., et al. (2022). Active back-arc thrust in North West Java, Indonesia. *Tectonics*, 41, e2021TC007120. <https://doi.org/10.1029/2021TC007120>

Received 22 OCT 2021

Accepted 23 JUN 2022

Author Contributions:

Conceptualization: Sonny Aribowo, Laurent Husson, Danny H. Natawidjaja, Christine Authemayou

Formal analysis: Manon Lorcery

Funding acquisition: Sonny Aribowo, Laurent Husson

Investigation: Sonny Aribowo, Laurent Husson, Danny H. Natawidjaja, Mudrik R. Daryono, Anggraini R. Puji, Astyka Pamumpuni, Dadan D. Wardhana, Gino de Gelder, Didiek Djarwadi

Methodology: Sonny Aribowo, Laurent Husson, Danny H. Natawidjaja, Christine Authemayou, Mudrik R. Daryono, Pierre G. Valla

Supervision: Laurent Husson, Danny H. Natawidjaja, Christine Authemayou

Visualization: Sonny Aribowo, Christine Authemayou, Mudrik R. Daryono, Gino de Gelder

Writing – original draft: Sonny Aribowo

© 2022 The Authors.

This is an open access article under the terms of the [Creative Commons Attribution-NonCommercial License](https://creativecommons.org/licenses/by-nc/4.0/), which permits use, distribution and reproduction in any medium, provided the original work is properly cited and is not used for commercial purposes.

Active Back-Arc Thrust in North West Java, Indonesia

Sonny Aribowo^{1,2} , Laurent Husson¹ , Danny H. Natawidjaja² , Christine Authemayou³ , Mudrik R. Daryono², Anggraini R. Puji², Pierre G. Valla¹, Astyka Pamumpuni⁴, Dadan D. Wardhana², Gino de Gelder¹, Didiek Djarwadi⁵, and Manon Lorcery¹

¹Institut des Sciences de la Terre (ISTerre), Université Grenoble Alpes, CNRS, Grenoble, France, ²Research Center for Geological Disaster, National Research and Innovation Agency (BRIN), Bandung, Indonesia, ³LGO, IUEM, CNRS, Université de Brest, Plouzané, France, ⁴Bandung Institute of Technology (ITB), Bandung, Indonesia, ⁵Indonesian Society for Geotechnical Engineering, Jakarta, Indonesia

Abstract The Java Back-arc Thrust scars the entire back-arc area of Java Island, but the faults' nature, timing, and activity remain partly elusive. Characterizing the structure and activity of the seismogenic Java Back-arc Thrust (historical earthquakes up to 7 M_w) is a cornerstone to evaluate associated geohazards. We focus on the western part of Java Back-arc Thrust that reaches the megalopolis of Jakarta. We combine morphotectonic data, seismic reflection, electric resistivity profiles, kinematic, structural field measurements, paleoseismological trenching, and sediment dating (optically stimulated luminescence and ^{14}C). Our results suggest that the interplay between the faults, volcanoes, and sedimentary basin modulates the propagation of the fault system across and along-strike. The West Java Back-arc Thrust has been active from Pliocene to Recent, but with a laterally variable tempo and tectonic regime. While tectonic activity was sustained for longer times in the eastern part, the West Java Back-arc Thrust broke through the Jakarta Basin in the west, possibly only since the Late Pleistocene, and partitions into a network of immature transpressive structures. We conclude that the West Java Back-arc Thrust has a high seismic hazard that requires a careful risk evaluation along its trace, as it threatens the numerous infrastructures of the densely populated West Java.

1. Introduction

The curvature of the Java-Banda subduction zone, from Sumatra to the Lesser Sunda Islands (Bali, Lombok, Sumbawa, Flores, and Sumba) and across Java yields an important spatial variability in deformation accommodation within the upper plate (Figure 1). In the west, the oblique subduction at the front of Sumatra is partitioned between the subduction and the dextral Sumatran Fault Zone (e.g., McCaffrey, 2009). In the northern part of the Lesser Sunda Islands, where convergence is normal to the trench, folds and thrusts accommodate shortening of the Flores Back-arc (e.g., McCaffrey & Nábělek, 1987). Between these two regions lies the Java Island, whose tectonic regime at the transition between the two domains is less clear. The island is the locus of intense volcanic and seismotectonic activity (Hutchings & Mooney, 2021). Yet, its tectonic structure received less attention than the other islands of the arc, despite the fact that the western part of Java is the most densely populated part of Indonesia. Specifically, it hosts the megalopolis of Jakarta, where the seismotectonic activity is even less studied than other regions. The lack of seismotectonic studies in northern part of Java can partly be explained by the fact that it has not only suffered from major devastating earthquakes in the last 200 years but also because the morphotectonic expression in surface topography is subtler for Java than elsewhere along the arc. Along the island, convergence rates decrease from ~ 65 mm/yr in East Java to ~ 58 mm/yr in West Java (Koulali et al., 2017). Besides the subduction megathrust that accommodates most of the convergence, several active faults affect Java island inland (Figure 1), such as the transpressive Cimandiri (Arisbaya et al., 2019; Marliyani et al., 2016), Lembang (Daryono et al., 2019), and Opak (Walter et al., 2008) Faults. However, E-W trending compressional faults are less documented in spite of the seismogenic risk. The most representative feature is the so-called Baribis-Kendeng Fault System (BKFS) that runs from East to West Java (Clements et al., 2009; Smyth et al., 2005). Here, we rename the BKFS as the “Java Back-arc Thrust” (JBT), which encompasses all sub-continuous E-W trending structures that strike Java more comprehensively than the concatenation of two more local names.

The JBT fault system may stem from the Flores Back-arc Thrust, which is the source of the 2018 M_w 6.9 earthquake series in Lombok (Yang et al., 2020), and the 1992 M_w 7.8 Flores earthquake (Beckers & Lay, 1995; Yeh et al., 1993). This fault propagates westward (Silver et al., 1983), as revealed by the 1976 M_w 6.5 earthquake reported in Bali (Ekström et al., 2012; Leimena, 1979) and an earlier damaging earthquake in the northern part

Writing – review & editing: Sonny Aribowo, Laurent Husson, Danny H. Natawidjaja, Christine Authemayou, Mudrik R. Daryono, Anggraini R. Puji, Pierre G. Valla, Astyka Pamumpuni, Dadan D. Wardhana, Gino de Gelder

of Bali (Nguyen et al., 2015; Wichmann, 1918). Further west, the Flores Thrust is thought to discontinuously join the back-arc thrust system of Java Island (Simandjuntak & Barber, 1996), across the two sets of fold-thrust belts in the Madura Strait (Ran et al., 2019; Susilohadi, 1995), and ultimately links to the JBT (Clements et al., 2009; Koulali et al., 2017; Simandjuntak, 1992; Simandjuntak & Barber, 1996; Smyth et al., 2005). The global scale model shows that the JBT is the youngest episode of the back-arc thrust propagation toward the west due to the Australian collision that enters Java Island (Husson et al., 2022).

In West Java, a conceptual model of northward thrust systems well explains thrust development over time (Clements et al., 2009). However, it might be that the model configuration is slightly different toward the east where the 5.5 M_w 1990 earthquake occurred (Figure 1b). Furthermore, the model East Java model provides a better explanation of the interplay between magmatic and thrust structures (Lupi et al., 2022) and volcanic loading (Smyth et al., 2005). In this study, we also model the northward propagation of the West Java Back-Arc Thrust (WJBT) around the epicenter of the 1990 earthquake in southwestern Cirebon.

The seismotectonic activity becomes less intense from the Flores Back-arc Thrust westward as it enters Java Island (Figure 1b). Nevertheless, reported local earthquakes attest to the potential hazard of the JBT. The focal mechanism of the 2018 M_w 6.0 earthquake east of Surabaya reveals N-S compression (Ekström et al., 2012). In central Java, the 1990 5.5 M_w thrust focal mechanism solution and 2020 4.5 M_w strike-slip focal mechanism recorded in the southern of Cirebon (Ekström et al., 2012) also reveals active deformation in the JBT. At the western end of Java, the JBT triggered the 1780 M_w Batavia (Jakarta) earthquake (Nguyen et al., 2015), which was the most disastrous earthquake reported in West Java (Albini et al., 2013). It destroyed houses near Jakarta (Wichmann, 1918), the brattle of which was heard from the Salak Volcano and Gede Volcano to the south of Jakarta (Harris & Major, 2017). Furthermore, the focal mechanisms of smaller magnitude earthquakes in West Java (Supendi, Nugraha, Puspito, et al., 2018, and BMKG catalog) reveal both N-S compression and strike-slip faulting (Figure 2a).

Geodetic data suggest that major east-west trending structures in the northern part of Java are active and sub-continuous across Java (Koulali et al., 2017) (Figure 1b). Block tectonic inversion of GPS data yields a transpressive slip rate on the JBT of ~ 5 mm/yr (Koulali et al., 2017). Likewise, continuous inversion of geodetic data (Gunawan & Widiyantoro, 2019) reveals widespread compression in North Java. More specifically, dilatation rates between Cirebon and south Jakarta reveal compression and shearing.

Overall, active crustal deformation, historical seismicity and geodetic data in NW Java undoubtedly attest to an active transpressive tectonic regime. However, not only the location and the geometry of the structures remain undefined, but also their tectonic activity. Importantly, the fundamental elements that are needed to characterize the JBT are getting more and more tenuous toward West Java. Yet, while it follows from historical seismicity that seismic hazard might be important, risk assessment in the densely populated region of West Java (including Jakarta) is in crucial need of such information.

In order to bridge the gap, we present new geological arguments to reappraise the tectonic activity and mechanism of the western end of the JBT, based on a combined structural, morphotectonic, paleoseismological, and seismic analysis. We focus on potential fault activity in West Java, north of the Cimandiri and Lembang Faults, which locally affect recent sedimentary deposits. We refer to this fault system as the WJBT as a substitute to inconsistent names such as Baribis Fault (Gunawan & Widiyantoro, 2019), Barabis Fault (Simandjuntak & Barber, 1996), and Barbaris Thrust (Clements et al., 2009).

2. Geological Setting of West Java

The northern part of West Java is mostly covered by two sedimentary platforms; the Java Northern Platform and the Bogor Trough further south (Figure 2a and Abdurrokhim & Ito, 2013; Martodjojo, 1984; Van Bemmelen, 1949). The northern platform consists of Quaternary alluvium and coeval volcanic deposits, the Tambakan and Gintung Formation (Kloosterman, 1989) that almost entirely cover northern Java and were deposited above the Pliocene Cisubuh, Late Miocene Klapanunggal Limestone, Middle Miocene Cibulakan claystone, Early Miocene Baturaja Limestone, and Oligo- Miocene Talangakar shale and Jatibarang volcanics (Figure 2b and Bishop, 2000; Putra et al., 2016). The Bogor Trough is filled up with turbiditic sedimentation and spans from Bogor to the south-eastern part of Cirebon. The sedimentary formations in the Bogor Trough have concomitant and occasionally

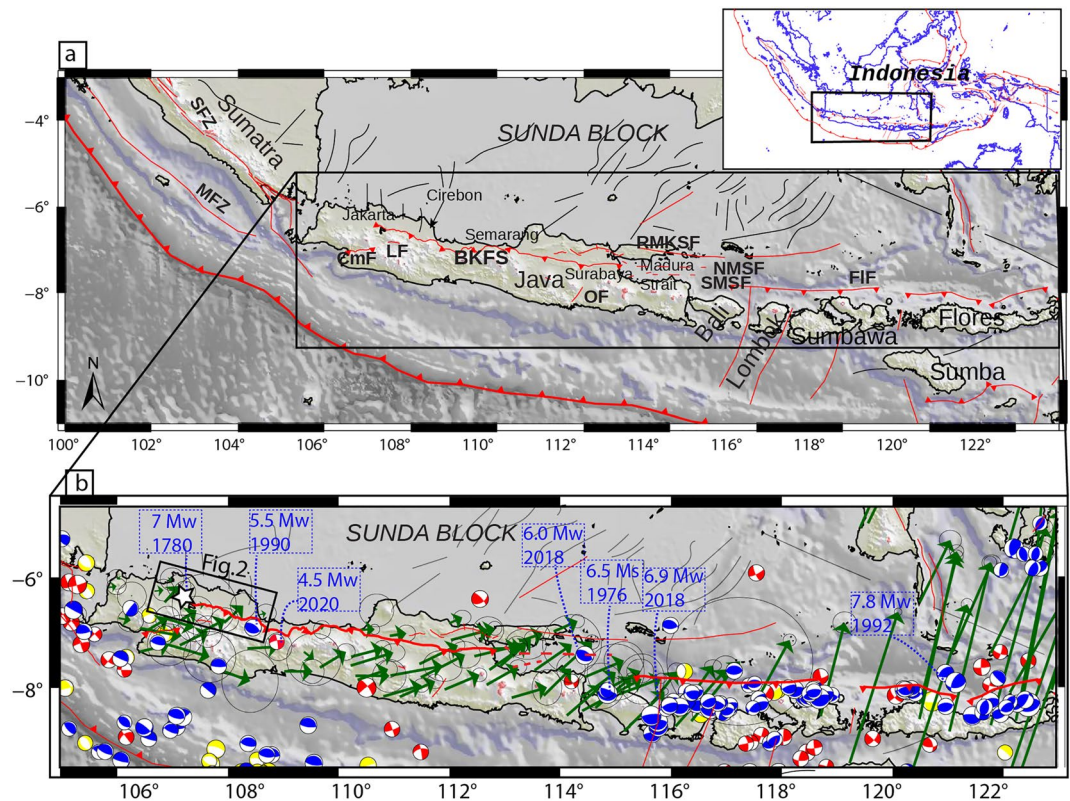


Figure 1. (a) Structural map of the Central Sunda Arc; red lines are active faults compiled from the Center of Earthquake Study (Irsyam et al., 2020) based on published faults such as the SFZ, Sumatran Fault Zone (Natawidjaja, 2018; Sieh & Natawidjaja, 2000); UKF, Ujung Kulon Fault (Mukti, 2018; Natawidjaja, 2018); CmF, Cimandiri Fault (Marliyani et al., 2016); LF, Lembang Fault (Daryono et al., 2019); FIF, Flores Back-arc Thrust Fault (Silver et al., 1983; Simandjuntak & Barber, 1996); OF, Opak Fault (Saputra et al., 2018); TF, Tulungagung Fault; RMKSF, Rembang-Madura-Kangean-Sakala Fault; NMSF, North Madura Strait Fault and SMSF, South Madura Strait Fault (Ran et al., 2020; Susilohadi, 1995); BKFS, Baribis Kendeng Fault System. Thin black lines are the Paleogene faults (Darman & Sidi, 2000). (b) Seismotectonic map with a zoom-in view to Java and the Lesser Sunda Islands (extent shown in panel A), displaying focal mechanism of thrust (blue), strike-slip (red) and normal faults (yellow) of the Central Sunda Arc shallow earthquake (~35 km depth, Ekström et al., 2012) and GPS velocities map (arrows in green) with respect to the Sunda Block (Koulali et al., 2017). The white star indicates the hypocenter of the modeled 7 M_w Batavia earthquake (Nguyen et al., 2015).

confusing regional names. Sedimentary rocks around Jatiluhur are found in the Miocene-Pliocene Subang Formation and Middle Miocene Jatiluhur Formations, these formations being covered by Holocene alluvium and volcanic deposits (Abdurrokhim & Ito, 2013). The region of Subang to Majalengka contains the Pleistocene Tambakan breccia, Pleistocene Citalang, Plio-Pleistocene Kaliwangu, and Miocene Subang Formations. The southern part of Cirebon-Kuningan (Cisanggarung, Figure 2b) comprises the Pleistocene Gintung, Pleistocene Cijolang, Plio-Pleistocene Kalibiuk, and Miocene Halang Formations (Puspaningrum et al., 2020).

Volcanic activity has been recorded in Java Island since the Late Eocene to Oligocene when the Old Andesite Formation was developed (Van Bemmelen, 1949). From the Upper Miocene onwards, volcanism gradually shifted to the north (Clements et al., 2009; Hall et al., 2007; Setijadji et al., 2006; Smyth et al., 2005).

Van Bemmelen (1949) first mentioned a physiographic boundary between the sedimentary rocks in the Bogor Trough, which runs from Bogor to Kuningan, and the sedimentary rocks of the northern platform of Java. Martodjojo (1984) later described the Baribis thrust fault as separating the two sedimentary units. The fault location from Bogor to Kuningan was refined by Simandjuntak (1992), who suggested that the Baribis Fault connects to the Kendeng fault in East Java and could be the lateral prolongation of the Flores Back-arc Thrust to the west of Java Island. Overall, the WJBT brings the volcanic arc up over the Sunda Shelf intermittently since the Miocene (Clements et al., 2009), while the shelf undergoes subsidence movements that constantly modify the geometry of the basin (Sarr et al., 2019; Zahirovic et al., 2016).

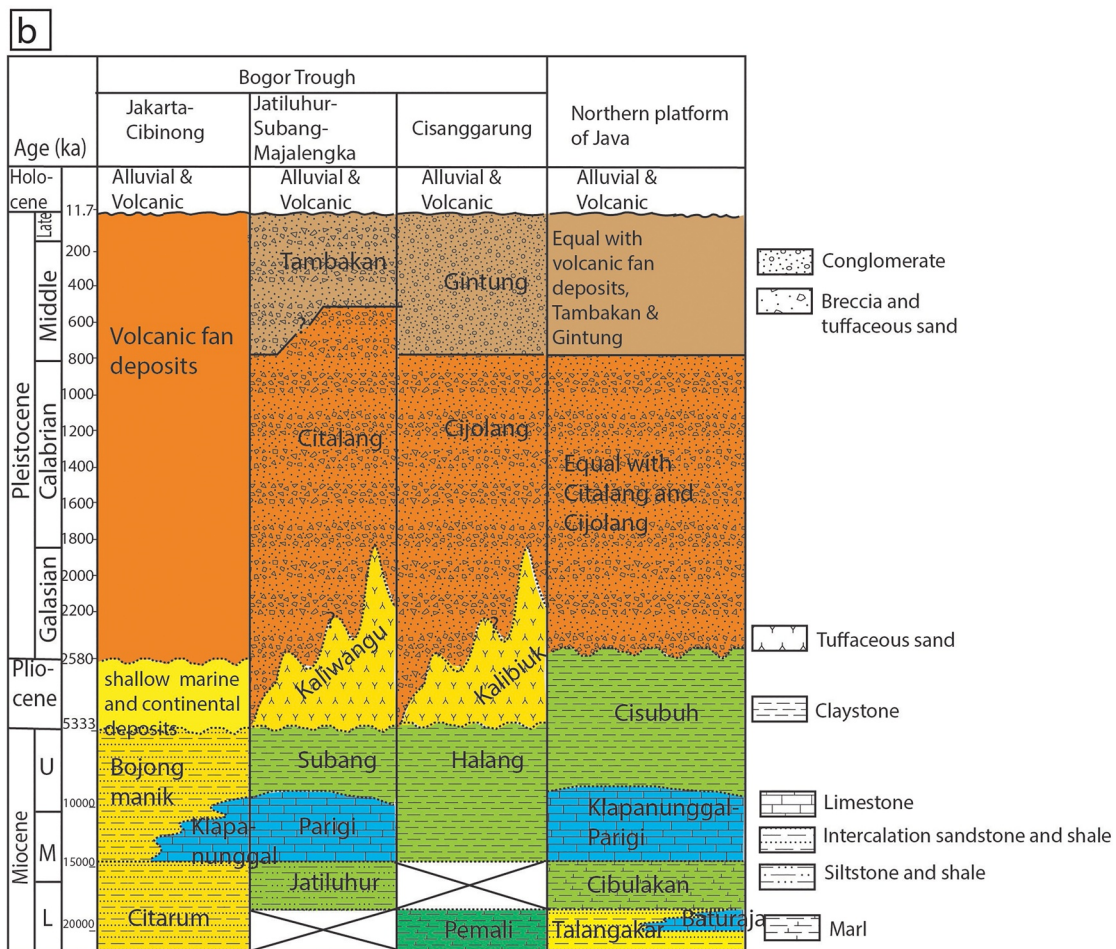
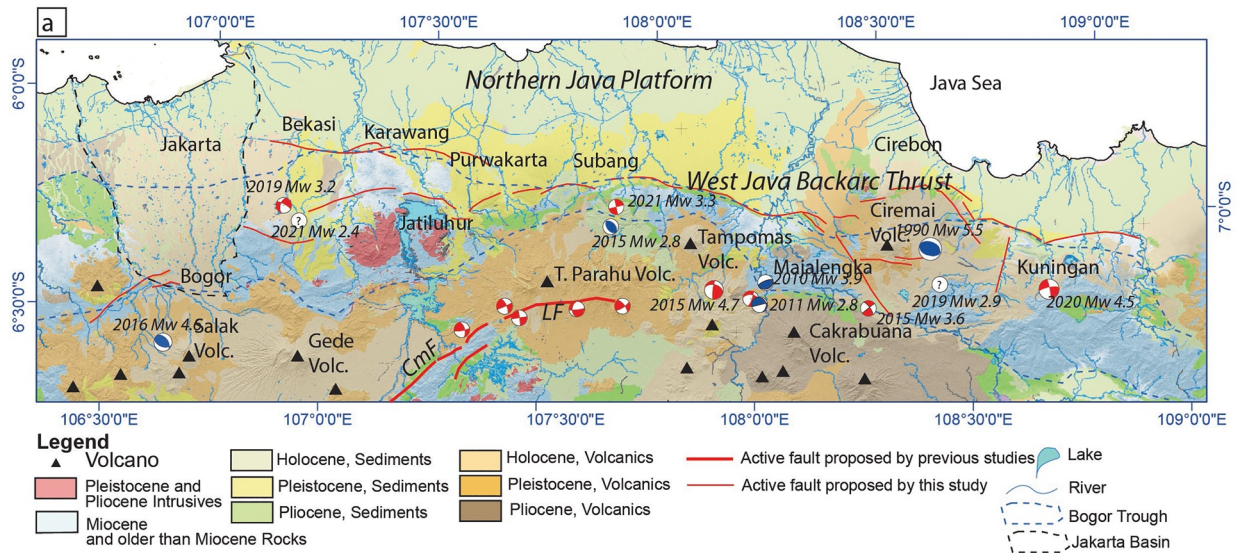


Figure 2.

This tectonic framework relates to the more general pattern of crustal deformation in Java Island and ultimately results from the convergence between the Indian and Eurasian plates. More precisely, E-W trending thrusts dominate in the northern part of Java (Koulali et al., 2017), while left-lateral structures are more distributed (McCaffrey, 1992). Regional thrusting in Java Island initiated during the Middle Miocene (Clements et al., 2009) and propagated northward during the Pliocene, suggesting a genetic link with the volcanic arc, which equally drifted northward during Pliocene (Clements et al., 2009; Van Bemmelen, 1949). Although the dynamics that relate those two primordial events are unclear, the last episodes of thrusting activity documented from the Late Pliocene–Early Pleistocene transition until present (Kloosterman, 1989) further reveal the relocation of the WJBT to the north of the volcanic arc (Figure 2a).

3. Data and Methods

3.1. Landscape Morphology and Surficial Fault Mapping

We mapped active faults to determine the surficial trace of the WJBT. Topographic scarps that affect recent sedimentary formations (Quaternary), and river offsets, show the landscape morphology over the fault. This method is commonly used to map active faults, for instance in Sumatra (Aribowo et al., 2017; Daryono & Tohari, 2016; Natawidjaja et al., 2017; Sieh & Natawidjaja, 2000), Java (Daryono et al., 2019; Marliyani et al., 2016), and Sulawesi (Natawidjaja et al., 2021). We use a blend of 30-m resolution SRTM topography images combined with 8-m resolution digital topography data called DEMNAS, 2-m resolution Pleiades images and spatial imagery. The observational dataset was occasionally complemented by drone surveys to improve the resolution of the digital elevation model (DEM).

3.2. Channel Steepness Index

We calculated the channel steepness index (k_{sn}) of the stream network to highlight slope ruptures that could be linked to vertical motion along the fault. We calculated the steepness index for each 100-m-long river segment (e.g., Castillo et al., 2014; Kirby & Whipple, 2012; Wobus et al., 2006). Under steady-state conditions, the slope S of fluvial channels can be conveniently reconstructed using a power-law relationship (Flint, 1974):

$$S = k_s a^{-\theta}, \quad (1)$$

where k_s is the steepness index, a is the upstream catchment area, and θ is the concavity index.

Because concavity varies among rivers and that variation leads to large changes in k_s , the steepness index is often expressed by its normalized form k_{sn} , by using the same reference concavity θ_{ref} for all channels being analyzed (Duvall et al., 2004; Kirby & Whipple, 2012; Snyder et al., 2000) such that:

$$S = k_{sn} a^{-(\theta_{ref})}, \quad (2)$$

where $\theta_{ref} = 0.45$ is a standard value in the literature.

We use the module Topotoolbox (Schwanghart & Scherler, 2014) from the MATLAB platform to produce the river profiles extracted from the 8-m resolution DEMNAS DEM. Since k_{sn} values increase drastically downstream knickpoints, they conveniently show up in river profiles and may be related to tectonic activity. This common method successfully permits locating, for example, the uplifted region of the Cimandiri Fault in Sukabumi, West Java (Marliyani et al., 2016). Issues can arise from the lithological effects, because laterally varying erodibility may result in spurious knickpoints that are unrelated to tectonics. To set apart tectonic knickpoints from lithological artifacts, we overlapped the k_{sn} map on the structural and geological map around two sites of observation (Cikamurang ridge and Cisanggarung hill, Figure 3a).

Figure 2. (a) Simplified geological map of West Java compiled from the Geological Survey Center-Indonesia (downloaded and modified from <https://geoportal.esdm.go.id/>) and the active faults in West Java. See the caption in Figure 1 for the references; the exception for the West Java Back-arc Thrust is based on our interpretation. The focal mechanism solutions for 2008–2014 were taken from Supendi, Nugraha, Puspito, et al. (2018), focal mechanism solutions for 2019–2020 were taken from BMKG (http://repogempa.bmkg.go.id/repo_new/). (b) Stratigraphic chart of West Java, the three locations show the stratigraphic of the area primarily discussed in the text (modified from Abdurrokhim & Ito, 2013; Puspaningrum et al., 2020).

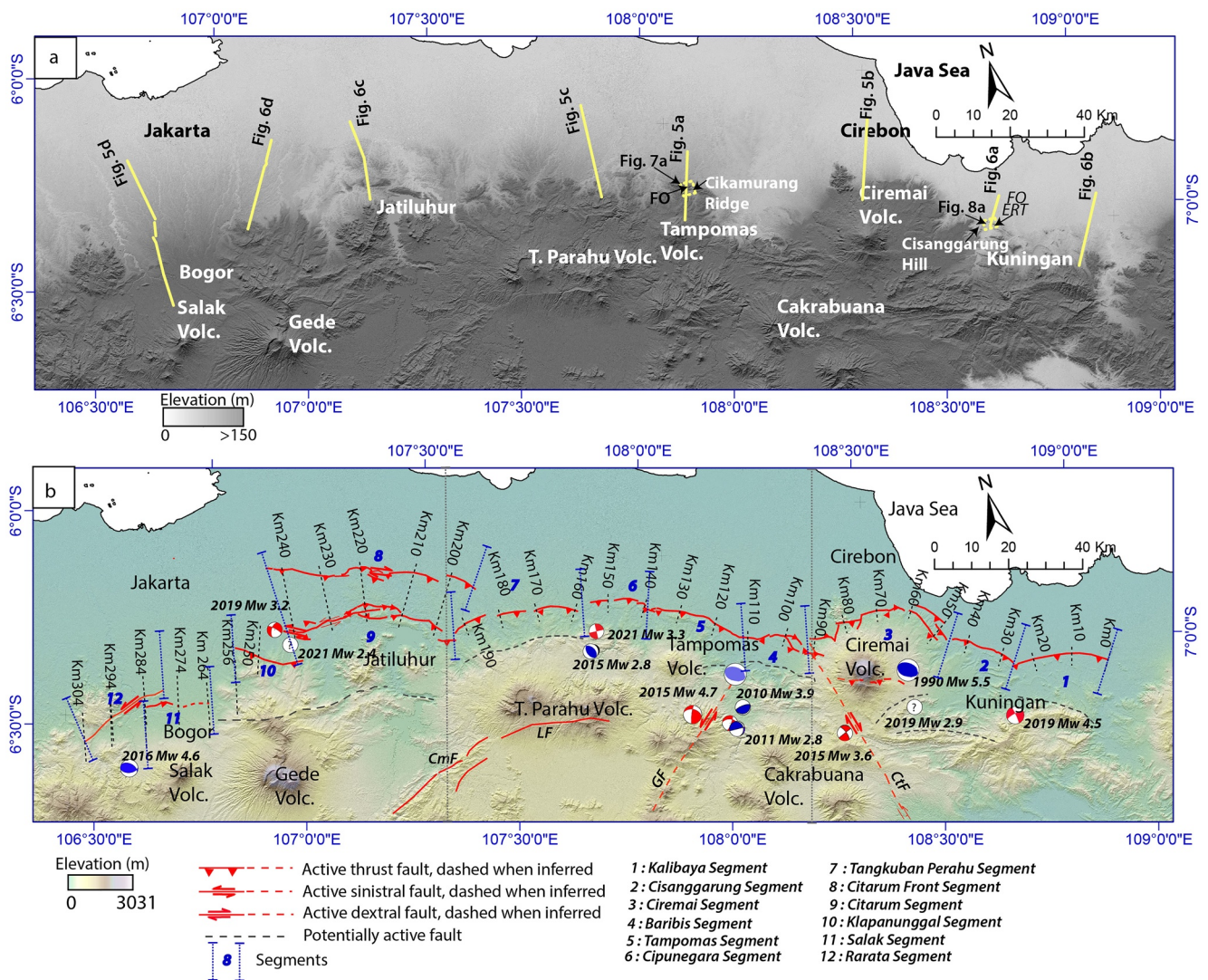


Figure 3. (a). Hill-shaded topographic map of northern west Java and the methods used in this study. Yellow bold lines represent the seismic location. FO, Field Observation; ERT, Earth Resistivity Tomography. (b) Active fault map showing 12 segments of the WJBT within three major regions. Gray dot vertical lines represent the boundary of the eastern, central and western regions. CmF, Cimandiri Fault (Marliyani et al., 2016); LF, Lembang Fault (Daryono et al., 2019); GF, Garsela Fault (Supendi, Nugraha, & Widiyantoro, 2018); CtF, Citanduy Fault (Simandjuntak & Barber, 1996).

3.3. Subsurface Data: Seismic Reflection

Seismic reflection profiles were acquired during the 1980s and 90s by the oil and gas industry and released by Data and Information Center, Indonesian Ministry of Energy and Mineral Resources (Pusatdin ESDM). These unpublished profiles, 60 in total for West Java, have an average length of approximately 25 km. They reach 5 s two-way-time, roughly corresponding to 4.5 km depth, assuming a mean propagation rate of 1800 m/s in the sedimentary cover of the platforms. We overlaid the swath profile (Pérez-Peña et al., 2017) on top of the seismic profile to see the topographic variations.

3.4. Structural Mapping and Paleoseismology—¹⁴C and OSL Dating

A detailed field study of Quaternary sedimentary deposits and fault mapping were performed to complete the structural map at selected locations. We first focused on the central part of the Cikamurang ridge in the north of Tampomas Volcano, and then on Cisanggarung hill, in the eastern part of Ciremai Volcano (Figure 3a). We preferentially investigated river channels that crosscut geological structures, allowing for the detection of the tenuous

Table 1
Sample Luminescence Detail and the Infra-Red Stimulated Luminescence (IRSL) Dating Results

Optically stimulated luminescence (OSL) sample	Radionuclide concentration							G2days (%per decade)	Age (ka)			
	Longitude	Latitude	Depth below surface (m)	K (%)	Th (ppm)	U (ppm)	Water content (%)					
O3	108.02773	6.66176	-15	1.15 ± 0.06	9.62 ± 0.48	1.79 ± 0.12	3 ± 2	2.34 ± 0.078	65.8 ± 2.7	11	5.65 ± 0.62	51 ± 5.3
O4	108.02772	6.66196	-10	1.37 ± 0.07	10.07 ± 0.5	1.97 ± 0.19	2 ± 2	2.69 ± 0.091	74.9 ± 3.3	13.8	6.33 ± 0.59	55 ± 7.4
BRB19.12	108.70449	6.93042	-1	0.85 ± 0.01	5.14 ± 0.24	1.45 ± 0.12	26.3 ± 5	1.41 ± 0.051	12.5 ± 1.8*	39.6	4.15 ± 0.66	12.8 ± 2.2

deformation of the most recent sedimentary layers and thus providing a temporal framework for the tectonic activity. Infrastructures on rivers also exposed outcrops of ~150 m length scale.

We carried out a paleoseismological approach to date paleoseismic events or tectonic activity. We focused on the slope break of the Cikamurang ridge, where the Cipanas River currently incises. The slope break is associated with the WJBT (Figure 3a). Current infrastructures give excellent N-S exposure to sedimentary outcrops, perpendicular to the trend of the fault, which allows for a thorough stratigraphic description of the sedimentary layers and fault networks. We used Quaternary dating methods with radiocarbon ¹⁴C and Optically Stimulated Luminescence (OSL).

¹⁴C dating is commonly well-known as an effective geochronological method for dating Holocene and late Pleistocene paleoseismological event (Grant Ludwig, 2015). To estimate sediment deposition times, we took radiocarbon (¹⁴C) measurements (Beta-Analytics) on dark-colored organic-rich material embedded in the sediment, as well as wood material within sediment deposits. The radiocarbon dates then calibrated using the SHCal13 calibration (Hogg et al., 2013).

OSL was performed to provide time constraints on sediment deposits that were subsequently affected by the fault activity. This dating method is reliable to date recent sediments within the range of 1–200,000 years (Rhodes, 2011). The principle of the OSL dating is to estimate the impact of environmental radiation on the crystalline structure of minerals in the forms of trapped electrons that can escape under exposure to natural daylight during sedimentation transport (e.g., Aitken, 1985). We collected three sediment samples from the observation sites (Table 1); two of them are from the paleoseismological trenching site (O3 and O4) and one from a fluvial deposit (BRB19.12) in the Cisanggarung River.

Sediment samples were taken with PVC tubes in the field with minimum light exposure. Then under subdued laboratory conditions (Institute of Geological Sciences, University of Bern), we removed carbonates and organic matters using HCl (32%) and H₂O₂ (30%). Sediment samples were sieved to grainsize fraction (180–250 μm) and Na-/Ca-feldspar fraction was extracted using density separation ($d < 2.70$, LST heavy liquids). Feldspar extracts were settled on 10-mm diameter stainless steel discs for subsequent luminescence analyses. Infra-red stimulated luminescence (IRSL) measurements were carried out using TL/OSLDA-20 Risø readers, equipped with a calibrated 90Sr/90Y beta source. Luminescence signals were detected using an EMI 9235QA photomultiplier tube, in the blue region through a Schott BG-39 and L.O.T.-Oriol D410/30 nm. We used a post-IRSL protocol (Lowick et al., 2015) with two successive IRSL stimulations at 50°C and 225°C to estimate sample equivalent doses. For BRB-19 sample, we used the first IRSL50 signal, but for the two other samples (O3 and O4), we used the post-IRSL225 signal given high fading values of the IRSL50 signal (Valla et al., 2016).

Fading causes age underestimations but can be measured over laboratory timescales, and the fading factor g (%/decade) can be used to correct feldspar age estimates. Fading corrections were calculated using the Luminescence R package (Kreutzer et al., 2012). All samples single-aliquots showed recycling ratios within 10% of unity and low residual doses. For final age calculation, we analyzed small-aliquot IRSL50 and post-IRSL225 De distributions (24 aliquots per sample) using the Central Age Model (CAM; Galbraith et al., 1999) or, in case of partial bleaching diagnosis as for BRB.19, using the Minimum Age Model (FMM; Galbraith & Green, 1990).

For all samples, around 500 g of the material was taken from the surrounding sediment for estimate of water content dose rate calculations, with specific activities of U, Th, and K using high-resolution gamma spectrometry (Preusser & Kasper, 2001). We assumed no internal K-content in Na-/Ca-feldspars (Valla et al., 2016) from mainly volcanic origin in the area. For final dose rate determination, we used the online calculator Dose Rate and Age Calculator (DRAC; Durcan et al., 2015). Concentrations were converted to infinite matrix dose using the conversion factors of Adamiec and Aitken (1988). The cosmic dose was calculated using present-day sample location and burial depth (Prescott & Hutton, 1994).

4. Results

4.1. Morphotectonics of the WJBT

The surface expression of the WJBT imprints the physiography in an east-west direction from north of Kuningan to north of Bogor (Figure 3). The topographic scarp is segmented, and it shows interplay with volcanoes in the southern part of the active fault. We divided the fault system into 12 segments within three major regions

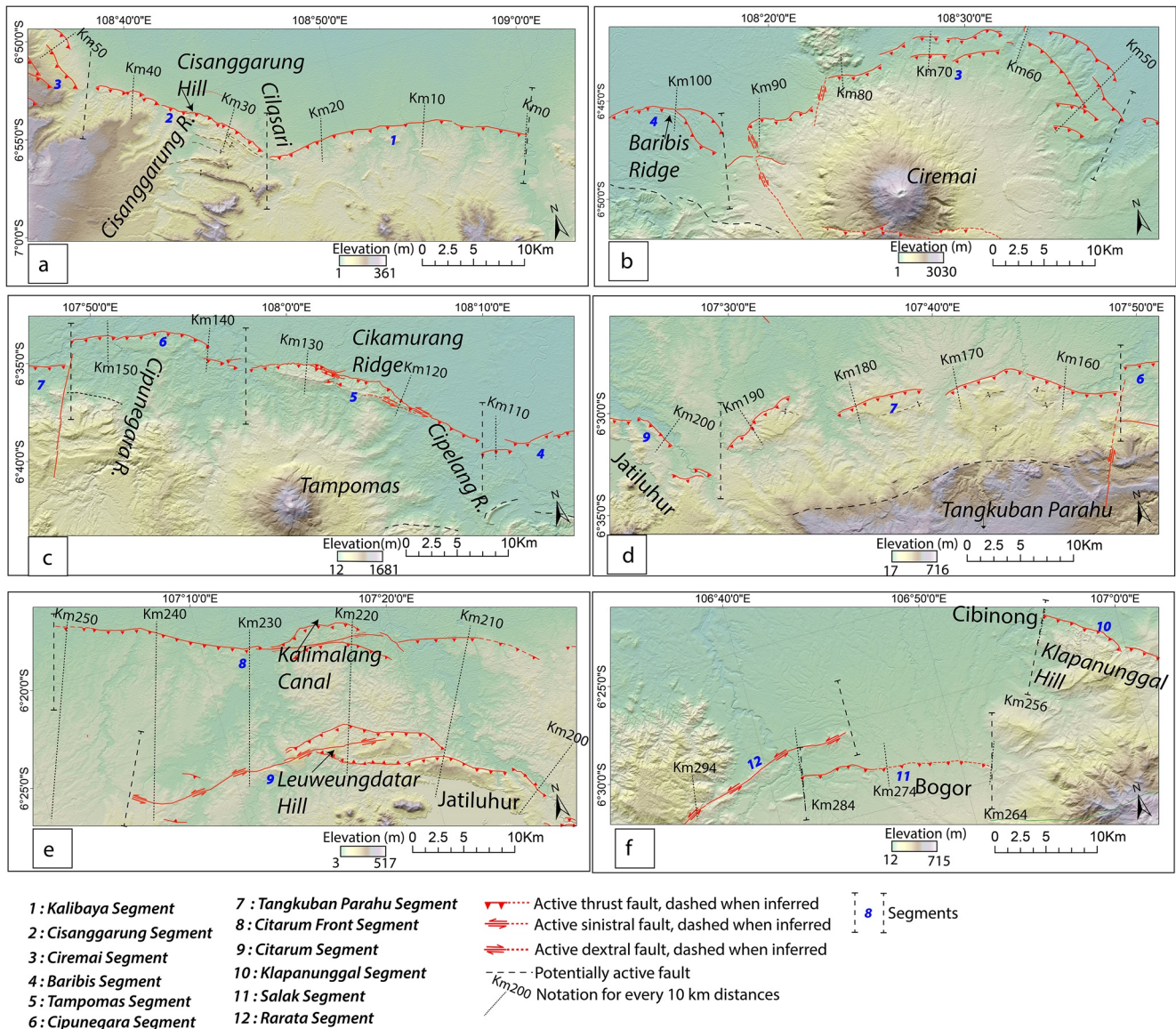


Figure 4. Zoomed-in view of the hill-shaded relief shows the active fault map of the eastern region (a) and (b), central region (c) and (d), and western region (e) and (f).

from east to west, based on the abrupt change of fault trends and the presence of relay zones. We labeled and named the segments after the names of active volcanoes immediately to their south, and, in the absence thereof, we named them based on the location of the topographic scarp or river name.

The eastern region comprises three segments that mostly wrap around the Ciremai Volcano. The E-W trending Kalibaya Segment is 25 km long. The lineament trace bounds the Holocene volcanic deposits in the south and the Holocene sedimentary deposits of the north Java platform. A small area of Miocene sediments outcrops in the easternmost part of the segment (Figure 2). The WNW-ESE trending Cisanggarung Segment has an 18 km long topographic scarp. The hanging wall is made of Pleistocene sediments and Holocene Ciremai volcanic deposits that outcrop as folded series in the eastern part, and are covered by the volcanic deposits in its western part (Figures 2 and 4a). The arcuate Ciremai Segment is 49 km long and marks the northern piedmont of the volcano (Figure 4b). The Ciremai Volcano southward deflects the segment geometry. In addition, the segment is truncated at some points by NNE-SSW-trending tear faults. We also identified a topographic scarp in the southern piedmont of the volcano that might correspond to a secondary fault. In the western part of the Ciremai Volcano,

we identified a NW-SE lineament that might correspond to the Citanduy Fault mentioned in a previous study (e.g., Simandjuntak & Barber, 1996), and possibly attested by an M_w 3.6 earthquake in 2015 with a strike-slip focal mechanism (Supendi, Nugraha, Puspito, et al., 2018). The 1990 M_w 5.5 earthquake with thrust focal mechanism was the highest magnitude recorded in the last 30 years around the Ciremai Volcano (Figure 3b).

The central region shows a sub-continuous fault trace that can be divided in several segments around the Tampomas and Tangkuban Parahu Volcanoes (Figure 3b). At its eastern edge, the tenuous topographic scarp of the Baribis ridge (Figure 4b) is ~ 14 km long and it is offset from the eastern segments. The hanging wall of the Baribis Segment consists of several folded hills. We interpreted a potentially active fault, based on the linearity of the topography, and supported by the published geological map (Djuri, 1995). To the south of the Baribis Segment, two shallow earthquakes with thrust fault mechanisms of magnitude 3.9 M_w and 2.8 M_w occurred in 2010 and 2011, respectively (Supendi, Nugraha, Puspito, et al., 2018). We suggest that those events are related to the Baribis Segment of the WJBT. The WSW-ENE fault scarp of the Tampomas Segment shows the clearest topographic scarp of the WJBT (although the Cipelang River partially erodes it), and is associated with the Cikamurang ridge (Figure 4c) 4.7 M_w sinistral earthquake that occurred in 2015 in the southern part of the region (Supendi, Nugraha, Puspito, et al., 2018). To the south, we also identified a NE-SW lineament that corresponds to the northern propagation of Garsela Fault (Supendi, Nugraha, & Widiyantoro, 2018). The E-W trending, 16 km long Cipunegara Segment was marked by a compressive earthquake of 2.8 M_w in 2015 (Supendi, Nugraha, Puspito, et al., 2018) and a strike-slip earthquake in 2021 with magnitude 3.3 M_w (Figure 4b). The 35 km-long topographic scarp of the Tangkuban Parahu Segment marks the end of a series of sub-continuous fault segments that end near Jatiluhur Lake (Figure 4d).

Last, in the western region, the fault trace is discontinuous at the surface. Although Martodjojo (1984) suggested that the fault stopped in Jatiluhur Lake, the geological map (Achdan & Sudana, 1992) suggests otherwise, revealing the existence of an active fault feature by an elongated hill (Marliyani, 2016). Indeed, surface morphology indicates that the fault continues westward and branches into two 50-km long segments, namely the Citarum segment to the south and the Citarum Front Segment further north. A ridge marks those segments to the north of Jatiluhur and a more tenuous morphological scarp around the Kalimalang Canal (Figure 4e). The Citarum Front Segment bounds the sediments of the northern platform of West Java to the north and the Miocene sediments to the south. In the southern part of the Citarum Segment, intrusions outcrop together with Miocene sedimentary rocks (Achdan & Sudana, 1992) (Figure 2a). The geomorphic expressions of the fault segments vanish westward. The short Klapanunggal segment shows the western continuation of the fault to the SW of the Citarum Segment. The Indonesian Meteorological, Climatological, and Geophysical Agency (BMKG) recorded two recent earthquake events at the western end of these segments. The 3.2 M_w 2019 earthquake has a sinistral focal mechanism, while the 2.4 M_w earthquake has no reported focal mechanism solution (Figure 3b).

Further west, to the south of the Jakarta Basin, discrete geomorphic indices of active faulting reveal at least local morphotectonic elements in the poorly resolved Salak and Rarata Segments (Figure 4f). Tracking recent fault activity is challenging due to the thick Holocene deposits produced by the Salak and Gede Volcanoes, covering both the Jakarta Basin and the Bogor Trough (Figure 2).

4.2. Regional Structure of the WJBT

To investigate the deeper structure of the fault, we interpreted a series of seismic profiles that run perpendicular to the fault trace. We overlaid the subsurface seismic profile with 5-km wide swath topographic profiles to show the relationships between the topographic scarp and the underlying structure (Figures 5 and 6). Seismic profiles along the northern part of West Java show the major southward-dipping fault that separates two different seismic facies.

We first consider a series of representative seismic lines that span well across the fault at different locations and image the interplay between the volcanic thrust and the sedimentation in the footwall (Figure 5). On the hanging wall, we interpret the ubiquitous chaotic facies as volcanic and volcano-clastic deposits. The facies of the footwall conversely features stacked sedimentary layers, tilted southward and thickening southward. Their facies bear powerful reflectors that alternate with lower-energy facies. One particularly low energy layer (e.g., Cik-U4) is commonly found in all sections. However, because we have no control points to assign a stratigraphic age at

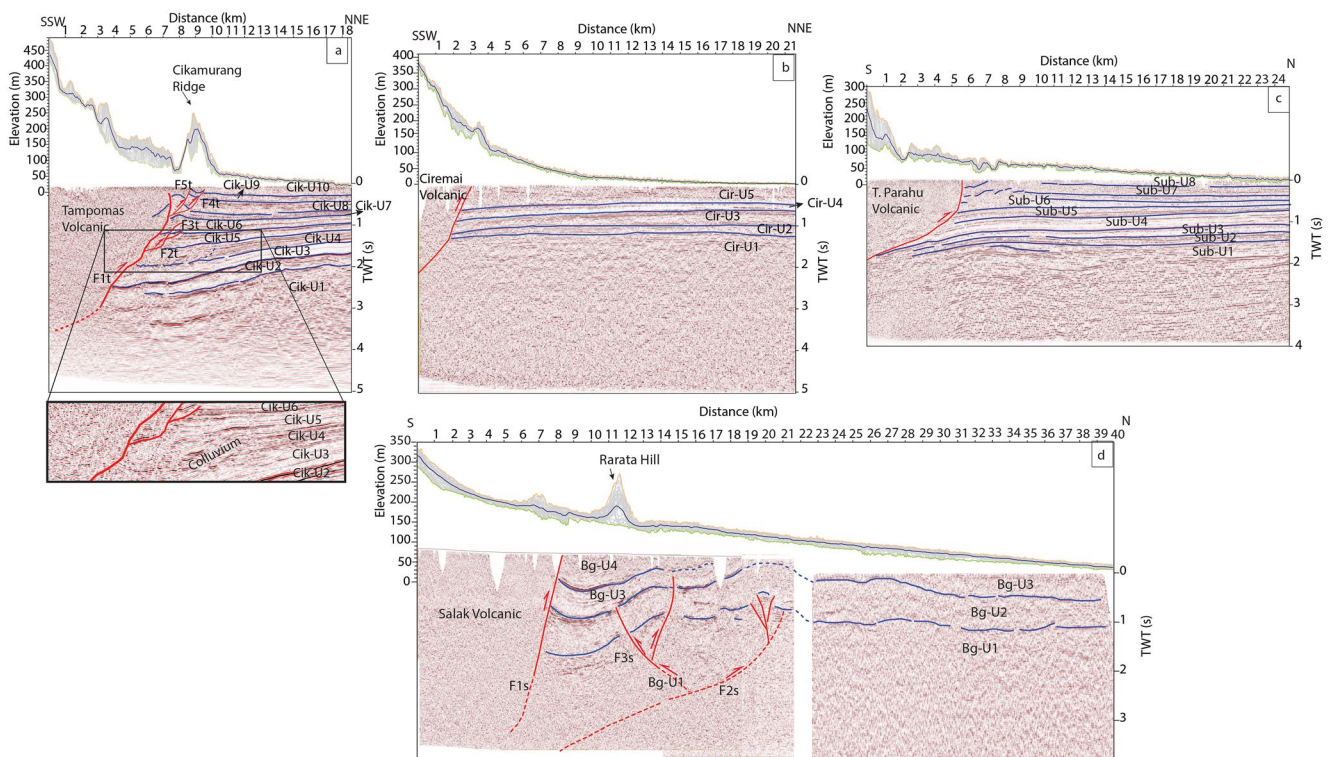


Figure 5. Topographic swath profiles and seismic reflection profiles of (a) Tampomas Segment, (b) Ciremai Segment, (c) Tangkuban Perahu Segment, (d) Salak Segment. Orange line of the topographic swath profiles represents the maximum value, the blue line represents the mean value, and the green line represents the minimum value. These seismic lines located immediately in the northern part of volcano edifices.

different locations, and because those lines are often too far apart, we do not attempt to correlate them and assign local names to the formations at given locations.

We start with the seismic profile across the Cikamurang ridge, in the central part of the WJBT, and that has a high-quality seismic profile that we use as a reference (Figure 5a). The location of the ridge immediately above the main fault confirms that the major south-dipping thrust is responsible for the fault scarp. Although the resolution decreases at depth, the listric fault suggests that it may be rooted on a deeper decollement level, possibly at ~ 4 s TWT (~ 3.6 km). The fault bounds two strikingly different facies. On the hanging wall, the southern facies shows chaotic reflection lines that we interpret as volcanic deposits of the Tampomas Volcano, in agreement with the geological formation at the surface (Figure 2). Occasional reflectors indicate that this unit may contain stratified volcano-clastic sediments interbedded within tuffs, ashes and lavas. The footwall's relatively flat reflection horizons reveal a stack of sedimentary units with a total thickness of up to ~ 3.9 s (~ 3.15 km). Based on their dip, facies, and the presence of unconformities, 10 sedimentary units have been individualized (Figure 5a). Cik-U2 and Cik-U7 to Cik-U10 do not show any change of thickness with a thickening toward the fault while Cik-U3 to Cik-U6 show a fan shape toward the fault.

The thrust has several branches (F2t, F3t, F4t, and F5t) to the north of the main segment (F1t) that reveal the spatial propagation of the deformation. F4t and F5t are superficial and propagate at the surface. In contrast, F2t and F3t are deeper, originating from the upper boundary of the Cik-U4 and are sealed by younger layers, which indicates that sediment deposition in the basin is syn-tectonic. In turn, the most conservative age interpretation for the uppermost layers is a Plio-Pleistocene age (Bishop, 2000), and a Holocene fault throw of several kilometers is unlikely. As such, we suggest that sedimentation, faulting, and volcanic activity were rather coeval. The latter point is also supported by more careful consideration of the seismic facies of the footwall: for instance, layer Cik-U4 exhibits laterally varying facies from well-layered sedimentary deposits in the north to a blurrier (yet still stratified) facies next to the fault (Figure 5a). We interpret this facies as a blend of sediments and volcanic colluvium, which attest to the simultaneous deposition of basin sediments and volcanic activity.

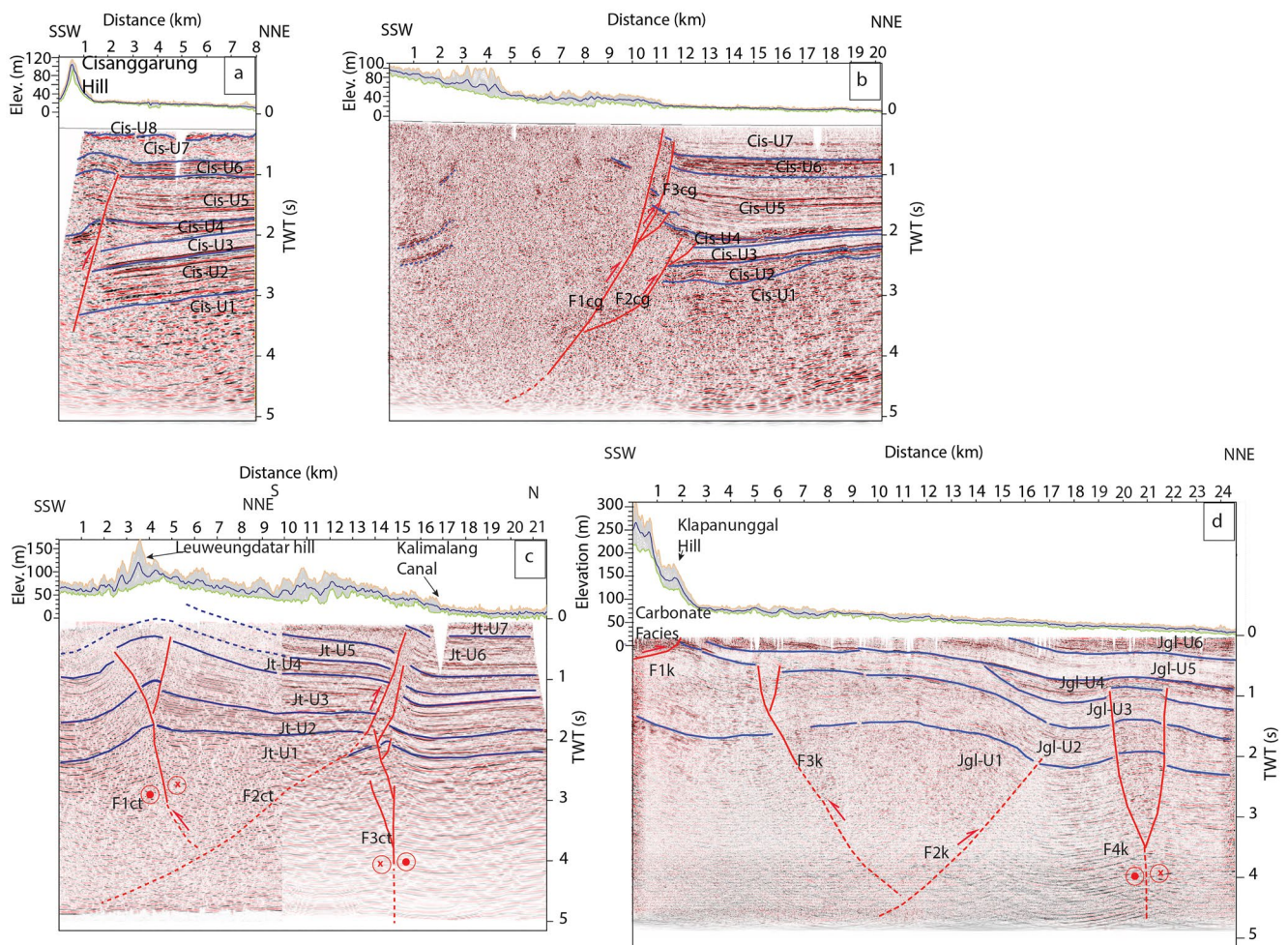


Figure 6. Topographic swath profiles and seismic reflection profiles of (a) Cisanggarung Segment, (b) Kalibaya Segment, (c) Citarum and Citarum Front Segments, (e) Klapanunggal Segment. The orange lines of the topographic swath profiles represent the maximum value, the blue lines represent the mean value, and the green lines represent the minimum value.

The seismic profile shows similar yet more condensed observations to the north of Ciremai Volcano (Figure 5b). The hanging wall is made of volcanic deposits. In the footwall, we interpreted five sedimentary units. Cir-U2 to Cir-U4 roughly shows a uniform thickness and are southward dipping, while Cir-U5 thickens southward. Likewise, volcanic deposits overthrust the basin deposits to the northeast of Tangkuban Parahu Volcano, where the surficial topography has a higher value in the southern part (Figure 5c, km2 to km5). The deeper sedimentary units (Sub-U1 to Sub-U3) are thinning southward, indicating that the depocenter was offset several kilometers from the fault. Layers Sub-U5 and Sub-U6 are thickening southward near the fault, while layers Sub-U7 and Sub-U8 are tilted northward and eroded. We interpret this behavior as the long-wavelength effect of the dynamic deflection of the basin geometry by mantle flow (Sarr et al., 2019; Zahirovic et al., 2016) rather than by a form of fault-related flexure, that would in principle only cause increasing subsidence toward the fault. Similar to reference Cikamurang section, some units (Sub-U5 to Sub-U8) show blurrier facies near the fault and vertical offsets of their boundaries that reveal the interplay with volcanic activity and the northward propagation of secondary fault segments.

Further west in the Bogor Trough, a steeply dipping thrust fault (F1s) overthrusts the Salak volcanic deposits onto the sedimentary deposits (Figure 5d). The topography does not show any clear topographic scarp, and the topographic deformation seems to be offset to the North, where the basin has been deformed. North of fault F1s, a large syncline is followed by a series of two small-scale antiforms. The deep structure of the northernmost fault (F2s) is a blind positive flower structure (approximately at a horizontal distance of 20 km). Between the two, the

Rarata hill is uplifted above a transpressive fault that we interpret to have developed from the back thrust (F3s) of fault F2s. The sedimentary units Bg-U2 and Bg-U3 do not show any thickness variation, nor any indication of syn-tectonic sedimentation, suggesting that the deformation postdates their deposition. This shows that the tectonic activity of the northern faults F2 and F3 is recent (post Bg-U4, i.e., Late Pleistocene to present) and that the structuration of the landscape is equally young. Overall, it indicates that the westward propagation of the WJBT from the more mature segments to the east of Jatiluhur is recent. Yet, the deformation of the sedimentary layer after their deposition is now substantial, which points to the seismic hazard that those tectonic structures may represent.

The second group of seismic profiles (Figure 6) images the structure across the fault. However, those lines are not located immediately in front of the volcanic edifices. Figure 6a shows the overlay between the topographic profile and the subsurface seismic profile located east of Ciremai Volcano (see location in Figure 3a). Unfortunately, the seismic data did not cross Cisanggarung hill (100 m high) southward. However, the seismic data presents a major tectonic discontinuity similar to a reverse fault in the southern part of the profile, affecting the lower units below and folding the upper unit. We interpreted eight sedimentary units, of which Cis-U1 shows high amplitude discontinuous layers. Above, it is overlain by Cis-U2 that comprises a continuous high amplitude reflector. Then, a low amplitude reflector of the Cis-U3 covers it. All these three deposits are southward dipping toward the fault discontinuity. The deposits then continue with Cis-U4. This unit shows a fan shape geometry with a thin continuous high amplitude reflector in the northern part, but then the reflector changed to low amplitude. We interpreted these layers as syn-tectonic colluvial deposits. The fault also deforms thick units of Cis-U5, Cis-U6 and Cis-U7 by folding, which fades out upward. Cis-U8 is in unconformity with Cis-U7.

We compare the seismic profile of the Cisanggarung Segment with a profile in the east. Across the Kalibaya Segment, the seismic profile (Figure 6b) shows clearly the structural boundary that separated the chaotic northern facies and a southern facies showing continuous reflectors. The southern facies between km3 and km11 of the profile shows a chaotic reflector that we interpret as volcanic deposits. In the southernmost part between km0 and km3, the reflector shows a southward dipping unit. The northern facies is composed of sedimentary units similar to the northern units of the western seismic profile (Figure 7a). We identified seven sedimentary units. The thrust system bounding the chaotic reflectors to the north (F1cg, F3cg) splays in different fault segments. The deepest secondary fault segment (F2cg) is blind and affect the deepest units (Cis U1 to Cis-U4). F3cg truncated all the sedimentary units except the upper part of Cis-U7.

Figure 6c shows a seismic profile in the northwest of Jatiluhur Lake (Figure 3). We interpret seven sedimentary units that we named Jatiluhur Unit 1 (Jt-U1) to Jatiluhur Unit 7 (Jt-U7). Jt-U1 is the oldest depositional unit in this profile. It shows a relatively horizontal layer offset by vertical fault (at km15, F3ct) that we interpret as a strike-slip fault. The thickness of Jt-U2 increases southward. The southern fault forms a pop-up structure that folds and offsets the layers. The structure at km4 (F1ct) is blind under the folded Jt-U4-U5 deposits, developing Leuweungdatar Hill's topographic high. The fault branches to fault F2ct offsets, the Jt-U1 and Jt-U7 and superficially forms the topographic scarp around Kalimalang Canal.

Westward, the seismic profile is located in the Km250 of the WJBT trace on a southern fault segment (Figure 3a). Here, the main active fault (F1k) does not have interplay with the volcanic deposits. The hanging wall consists of folded Middle to Late Miocene limestone beds (Turkandi et al., 1992) that are associated with the Klapanunggal Hill. The seismic line (Figure 6d) shows six units folded northward and a reverse fault dipping southward beneath km 2 (F1k). Beneath km19 and km22, the sedimentary layers of Jgl-U1 to Jgl-U3 are affected by thrusting F2k. Between F2k and F1k, the back thrust of the F2k (F3k) develops a positive flower structure that affects Jgl-U1 to Jgl-U3. The thickening layer of Jgl-U4 reveals syn-tectonic sedimentation. The units of Jgl-U5 and Jgl-U6 are folded, indicating that fault activity still occurred during the deposition of both units.

4.3. Structure of the Tectonic Front

We focus on two study sites within the central and eastern parts of the WJBT, where our detailed investigation revealed that the fault is outcropped to the surface. These sites offer good quality outcrops that permit observing the most recent activity of the fault.

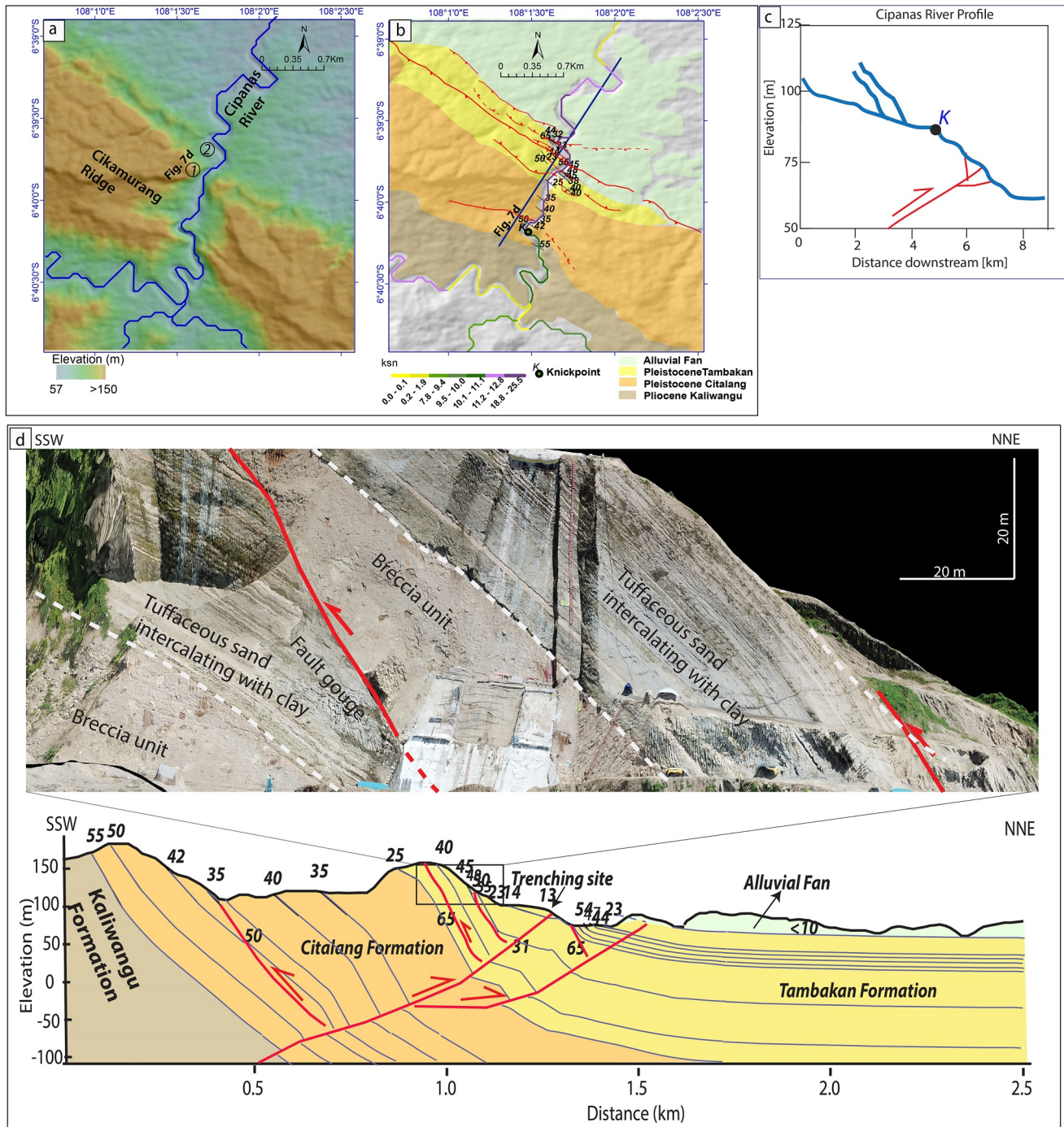


Figure 7. (a) Uninterpreted 8 m resolution DEM around Cipanas River, black lines show the location of the resistivity profiles. Circle number 1 shows the location of the northward dipping antithetic thrust outcrop (see Figure 7d). Circle number 2 shows the location of the paleoseismological trench (see Figure 9). (b) Detail active fault and geological map around Cipanas River combined with the channel steepness index value of the Cipanas River, the blue line shows the geological profile's location. (c) Cipanas river profile refers to the river flow on the map in Figures 7a and 7b. (d). Above: Mosaic photograph of the northward dipping antithetic thrust of the Baribis Fault Zone (see Figure 7a for the location). Bottom: Geological cross-section of the outcrops along the Cipanas River that crosscut the Cikamurang ridge. The italic numbers are dip values in degree.

4.3.1. Tampomas Segment

To the north of the Tampomas segment, the Cikamurang ridge is incised by the Cipanas river (see DEM Figure 7a) and exposes sedimentary layers that we interpreted as the Kaliwangu, Citalang and Tambakan formations. The

channel steepness index along the Cipanas River shows high k_{sn} values on the topographic scarp (Figure 7b). Similarly, the longitudinal river profile reveals a knickpoint with a 25-m high cliff above the fault trace (Figure 7c). The knickpoint is located within the Citalang Formation, which rules out the possibility of a lithological control on the location of the knickpoint.

A south verging thrust (N 330° E/65°) disrupts the series of northward dipping sediments of the lower part of the Tambakan Formation (Figure 7d). It puts the breccia layer to the top of the intercalated tuffaceous sandstone and brownish clay layer, and we interpret it as an antithetic fault. The dip of the sedimentary layers gradually decreases toward the foot of the ridge. The most recent sediments dip to the north at a very low angle, possibly attesting to the propagation of the fault. These structural observations are synthesized in a geological cross-section (Figure 7d) along the Cipanas River and across the Cikamurang ridge. The overarching structure is a northward propagating anticline. The fault is locally emerging and shows multiple secondary thrusts and back-thrusts. We show more details on the small-scale structure of this fault in the paleoseismological investigation (see Section 4.4).

4.3.2. Cisanggarung Segment

The second set of structural observations were collected along the Cisanggarung River (Figure 8a) which cross-cuts the eponymous Cisanggarung hill, with a 100-m topographic scarp that is half as high as that of the Cikamurang ridge. The channel steepness indices (k_{sn}) along the Cisanggarung River are low (Figure 8b). However, we can still observe a change to a high k_{sn} values, first in the northern part close to the approximate location of the blind fault identified by the seismic line and second across the Cisanggarung hill. The Cisanggarung River profile shows a second small knickpoint upstream of the fault, which attests to the faults' tectonic activity (Figure 8c).

From south to north across the hill, structural measurements (Figure 8d) show northward-dipping layers of the Upper Miocene Halang Formation, followed by the Pliocene to Pleistocene Kalibiuk and Pleistocene Cijolang Formations. A thin layer of the Gintung conglomerate and a more recent Gintung Formation unconformably cap these formations. Dip and strike measurements reveal a northward propagating anticline. The Halang, Kalibiuk and Cijolang Formations show very modest indices of syn-tectonic activity. An angular unconformity is visible in the Kalibiuk formation (Figure 8d), attesting to tectonic activity. Still, because the stratigraphic facies remains identical across the unconformity (shelly marine limestone), it shows a dynamic change in the geometry of the basin. An episode of pervasive tectonic activity postdates the deposition of the Cijolang Formation, as revealed by its important folding and the unconformity with Gintung Conglomerates. The conglomeratic layer dips to the north at a low angle (<5°), but is not yet crosscut by the fault, which suggests that the thrust is still blind, in agreement with seismic observations (Figure 5a).

4.4. Kinematics of the WJBT—Cisanggarung and Tampomas Segments

In Cisanggarung, chronologic constraints are limited, for we only OSL-dated a sand lens (BRB19.12) of Gintung Conglomerate at the front of the fault system (Figure 8d), yielding an age of 12.8 ± 2.2 ka BP. This conglomerate is slightly deformed and tilted northward, indicative of its tectonic activity during the Holocene.

North of the Cikamurang ridge, in the Tampomas Segment, we achieved a much more comprehensive overview of the fault kinematics thanks to the construction of a large infrastructure that exposes a ~150m-long and ~17m-high trench (Figure 9a, see location in Figure 7a) across the northernmost fault of the WJBT. We interpreted the stratigraphic and tectonic structures to evaluate the recent activity of the fault (Figure 9b).

We identified 10 depositional units mainly composed of tuffaceous sands of variable compositions and grain sizes (Figure 9c). Units U1, U2, U3, and U4 on the northern side of the trench, and units U1' and U2' on the southern side are primarily horizontal and have uniform thicknesses. A transpressive fault (F3) separates units U1, U2, U3 and U4 from units U1' and U2'. The relative chronology between the two groups is elusive. Unit 5 unconformably covers these units over an irregular interface that we interpret as erosive. These interpretations suggest that fault F3 was active during and after deposition of U4 and prior to the deposition of U5. Unit 5 is unconformably covered by unit U6, which bears three sub-units with contrasting lithologies and dip that we interpret as syn-tectonic sedimentation. Unit U7 shows south-dipping strata, and unit U8 shows a large south-verging overturned slumped anticline, likewise indicating syn-tectonic sedimentation. The unconformity above U4 and U2',

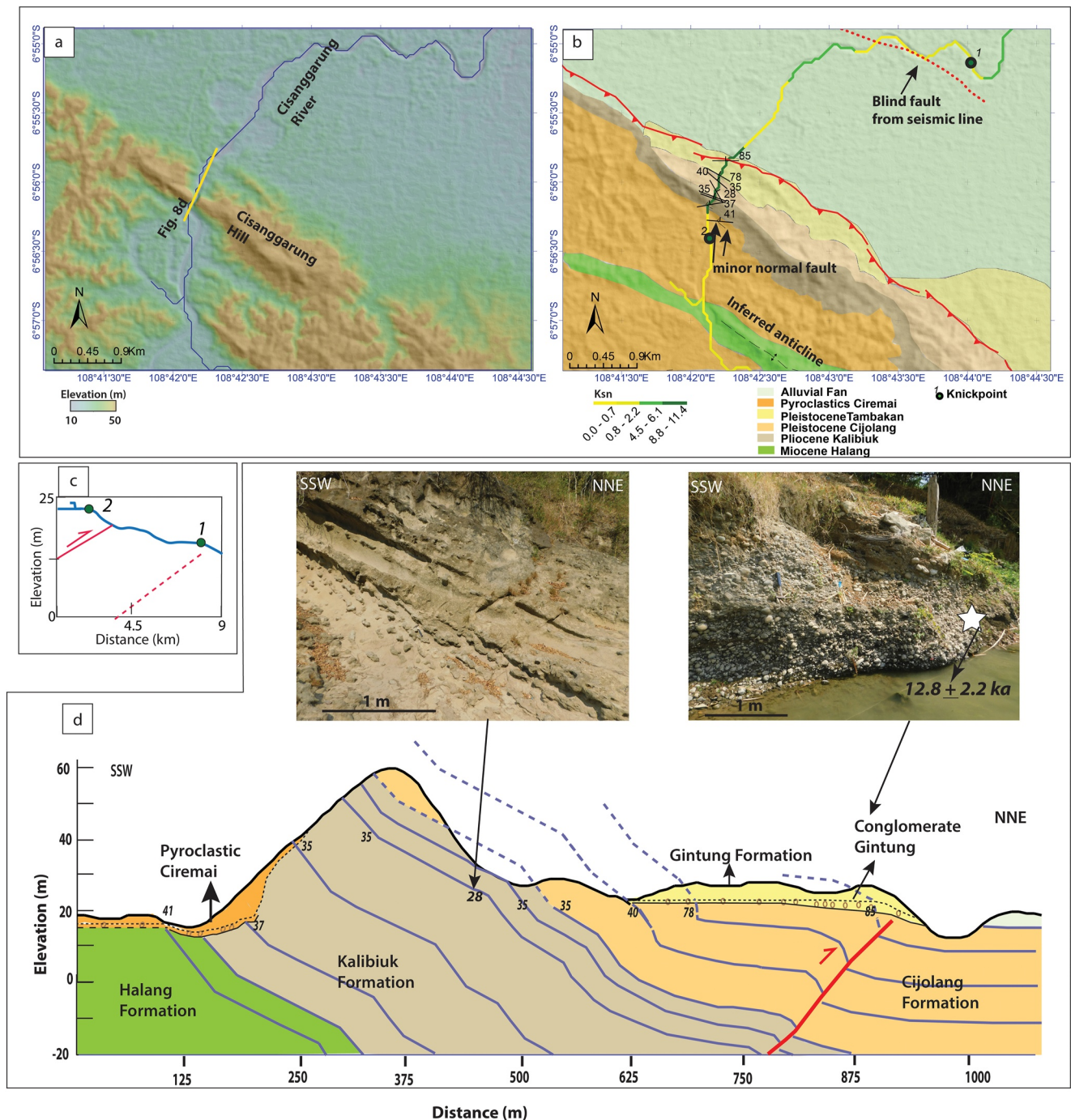


Figure 8. (a) Hill-shades Digital Elevation Model (DEM) image around Cisanggarung River. The black line shows the location of the resistivity profile, and the yellow line is the location of the geological cross-section. (b) Geological map of Cisanggarung River. (c) Cisanggarung river profile refers to the river shown in Figure 8a. (d) Geological cross-section of Cisanggarung River and outcrop photographs of the angular unconformity and sample location.

the lithological change, and layer dipping on both U4 and U2' boundaries with U5 indicate that the sedimentation dynamics changed from alluvial sedimentation (U1 to U4, U1' and U2') to colluvial sedimentation (U5 to U8).

OSL dating on sand lenses of U1' yields ages of 55.5 ± 7.4 ka and 51 ± 5.3 ka (Figure 9c). A wood fragment in the lower part of U6 has ^{14}C conventional radiocarbon age of 5330 ± 30 BP and corresponds with a corrected calendar year age of 6.1 ± 0.1 ka BP. A paleosol in U8 was ^{14}C dated to $7,720 \pm 30$ BP, corresponding to

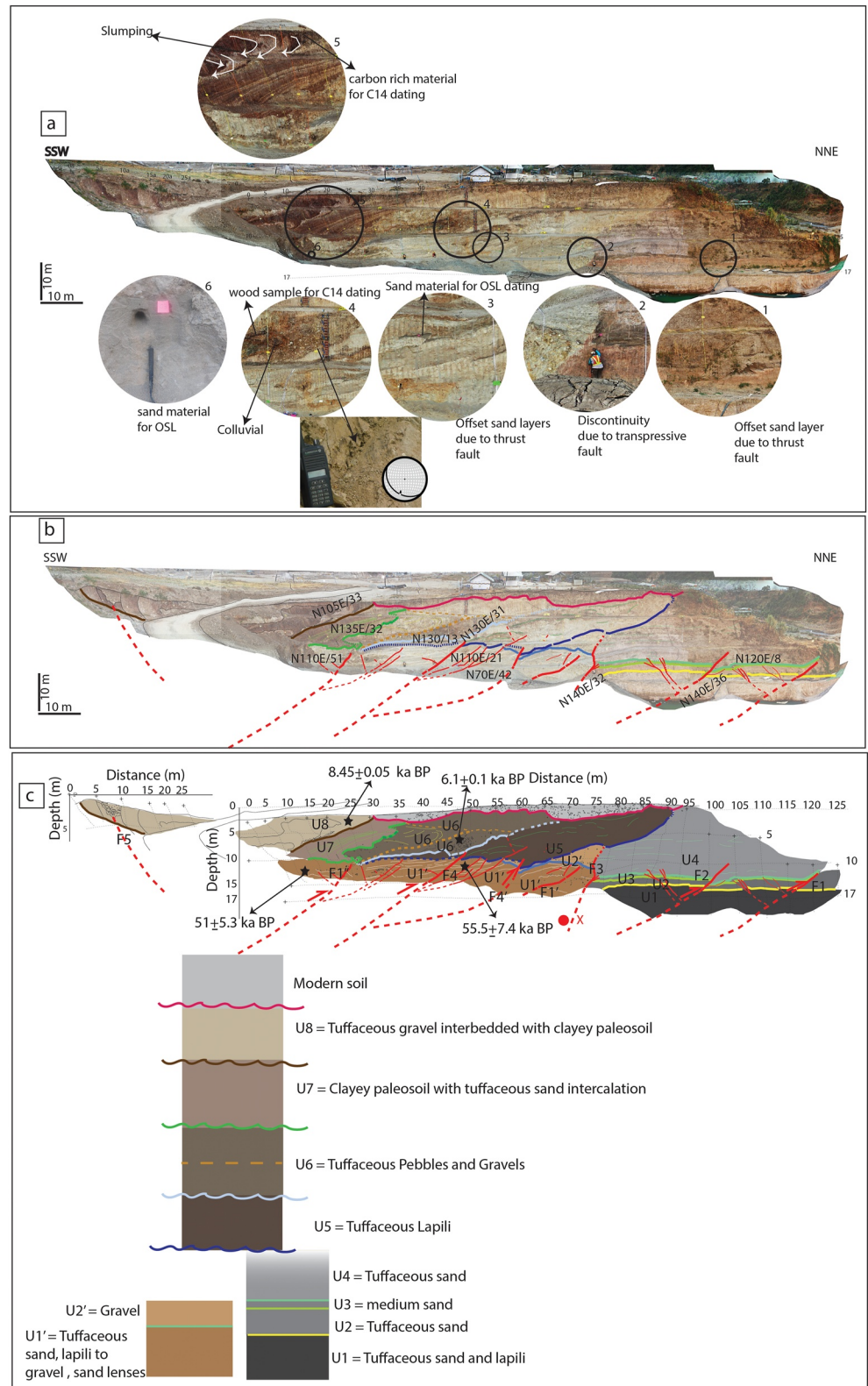


Figure 9. (a) Mosaic photograph of the paleoseismological trench (see Figure 7a for the location). (b) Interpretation of the sedimentary layer and the structure of the mosaic photograph of the paleoseismological trenching site. (c) Interpretation of the sedimentary layer with color and the structure from the mosaic photograph.

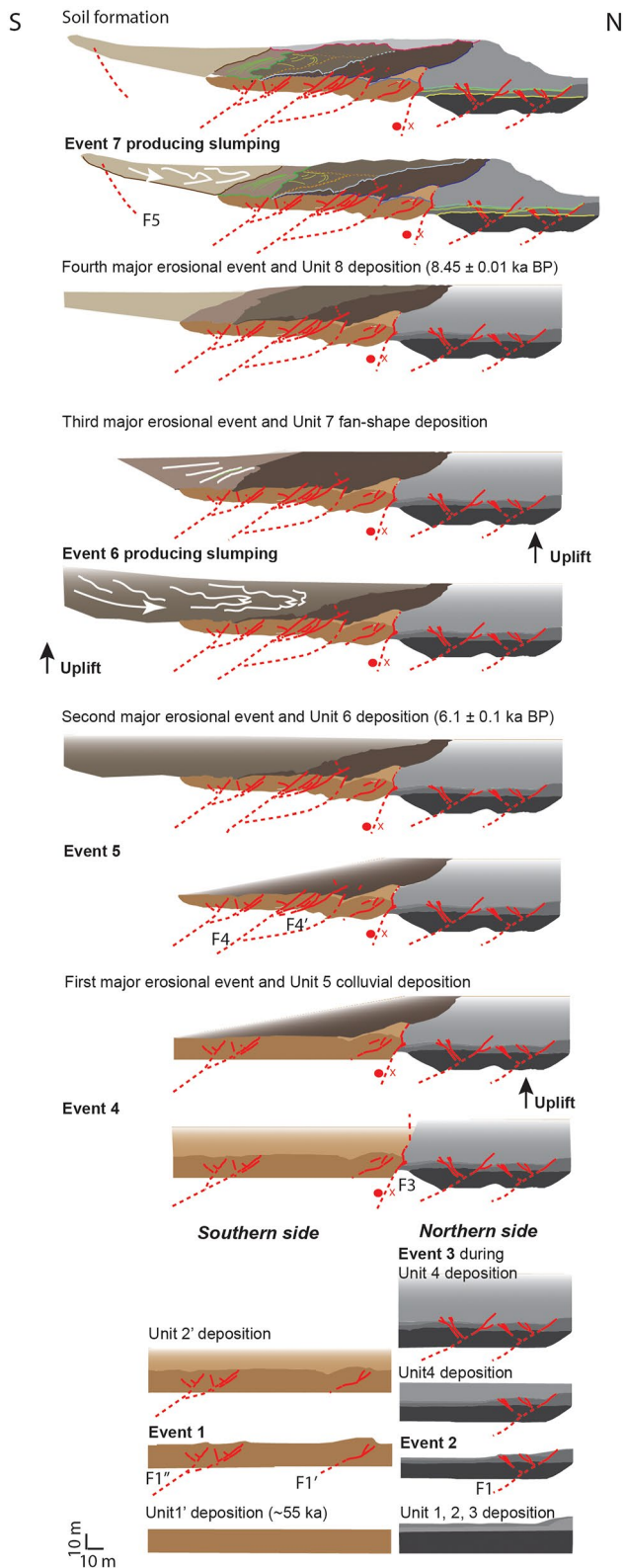


Figure 10. The inferred sequence of deformation and sedimentation at the trenching site.

calibrated calendar year age of 8.45 ± 0.01 ka BP. These ages indicate that the tectonic activity of F3 is recent (from Late Pleistocene to Holocene).

In addition, a range of south-dipping secondary thrusts (striking from 85° to 140° and dipping from 32° to 51° with pitch northeast vergence) disturb the stratigraphic series. Some are associated with back-thrusting that attest the back-thrusting also occurred locally, at the trench scale. We back stripped the tectonostratigraphic sequence based on our interpretation to unravel the kinematic history over the last ~ 60 ka (Figure 10). A first surface rupture event E1 is attested by F1' and F1'' that cut through U1' and are sealed by U2'. A second rupture event, E2, occurred between the deposition of U2' and U5. A rupture event E3 occurred southward between deposition of U3 and U4 (fault F1). Event E4 affected the bottom part of U4 and thus occurred during its deposition. Due to the lack of dating for U1-U5, we could not determine the rupture event ages between E3 and E4 with E1 and E2. E5 is associated with the main fault F3 and postdates the deposition of U4. E5 occurred during the sedimentation of U5 and prior to U6. Slumps infer E6 to have occurred during deposition of U6. Slope destabilization occurred during the sedimentation of U6 after the deposition of its lower detrital part at 6.1 ± 0.1 ka BP and before the deposition of U7. E7 is recorded by slumps in U8 and back-thrust fault F5. The U8 deposit has an age of 8.45 ± 0.01 ka BP, which is apparently older than the U6 deposit. This difference can be explained by potential age overestimation for U8 given that we collected carbon-rich soil material for bulk dating for U8 (whereas we collected wood material for U6). In addition, several slumping events occurred after the deposition of U6 that makes sequential chronology a bit confusing. However, the event E6 and F5 attest for the tectonic activities younger than 6 ka BP.

5. Discussion

5.1. Timing of Activity of the WJBT

Overall, our observations show that the WJBT deformed Pliocene to recent sediments, which globally frames the period of activity of the fault. Based on our observation, we propose a tectonic model of West Java that shows the northward propagation of the thrust in the back-arc domain and the interplay with the volcanic arc (Figure 11). The most recent back-arc thrust structure is located north of the Tampomas Volcano which is the northernmost volcano of the West Java Quaternary volcanic arc. Our study is consistent with earlier studies suggesting that thrusting in West Java was initiated after the Miocene (Clements et al., 2009). Starting with the Cimandiri Fault in the southern part of the modern volcanic arc and propagating northward with the onset of the Lembang Fault and the WJBT, later affecting the arc and back-arc areas (Clements et al., 2009; Hall et al., 2007).

The interplay between the fault and the volcanic arc has been suggested earlier (Clements et al., 2009; Martodjojo, 1984). While the surface deformation pattern indicates that the volcanic front interacts with the thrusts, seismic lines reveal the coeval and continuous interplay between volcanic activity, fault activity and sedimentation in the footwall, whose geometry jointly responds to crustal tectonics in Java and to the dynamic subsidence of the Sunda shelf (Sarr et al., 2019; Zahirovic et al., 2016). Consequently, the onset of thrusting probably dates back to the Pliocene migration of the volcanic arc. The WJBT would then be the most recent thrust fault of several thrusting episodes in Java Island (Hall & Smyth, 2008; Smyth et al., 2005).

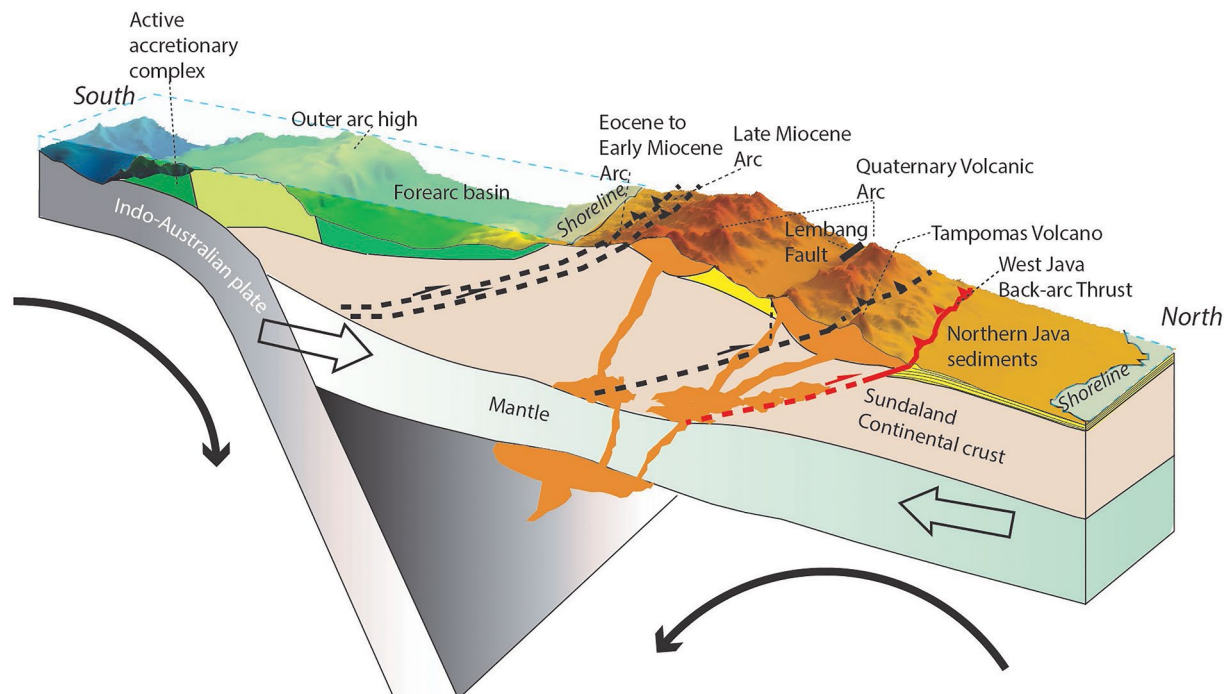


Figure 11. 3D tectonic model of the northward propagation of the volcanic arc and the West Java Back-arc Thrust. Red curve delineates the tectonically active WJBT.

This timing is consistent all along the WJBT east of Jatiluhur. The situation differs westward in the Jakarta Basin, for no active volcano triggered the tectonic propagation of the fault. The main Gede and Salak Volcanoes stand further south. It follows that thrust propagation was delayed with respect to the eastern counterpart of the WJBT. The delay of the northward propagation is evident from seismic lines that show little to no syn-tectonic sedimentation in the sedimentary basin. This indicates a very recent, Late Pleistocene northward propagation of the faults. The timing of onset, therefore, varies along the strike of the WJBT.

East of Jatiluhur, seismic lines indicate a sub-continuous tectonic activity, although syn-tectonic activity reveals that several periods of quiescence separated periods of sustained tectonic activity. The Holocene in particular was a period of sustained fault activity, as indicated by our geochronological data of tectonically deformed outcrops at two sites at the northernmost front of the WJBT. West of Jatiluhur, tectonic activity was active until recently, as revealed by the deformation of the uppermost sedimentary layers that affect the morphology on the surface. Last, several monitored and historical earthquakes attest for its current activity all along its strike.

5.2. Northward Propagation of the WJBT and Interplay With the Volcanic Arc

Volcanoes play a fostering role in the northward propagation of the fault as they localize thrusts. At a regional scale, this is attested by the fault bend that follows the envelope of the volcanoes; in particular, the southward deflection of the fault in the westernmost part is emblematic. Note that the relationship is possibly less weak than in the obliquely convergent part of the subduction of Sumatra (Acocella et al., 2018). However, volcanoes in both cases are located close to the fault. In Java, particularly, volcanoes are systematically located to the south of the fault and overthrust the basin.

At a more local scale, the curvilinear shape of the surficial trace of the faults indicates that the volcanic edifices control the geometry of the thrusts. The interplay is particularly obvious for the Ciremai, Tampomas, and Tangkuban Parahu Volcanoes, to the north of which the fault trace seems to have deviated. This suggests that volcanic activity may have precisely triggered the localization of the fault to the north of the volcanoes themselves (Figure 11). Seismic lines image the rooting of thrusts underneath the volcanoes. However, the dynamic interplay between the tectonic and volcanic structures occurs at a depth that is unfortunately beyond the resolution of the investigated seismic lines. Nevertheless, the determinant role of the volcanoes over thrust development is

indirectly highlighted when comparing the lateral variations of the deformation along the thrust (East of Jatiluhur, where the WJBT is mature), as the structure of the fault differs from one segment of the WJBT to another (Figures 5 and 6). We interpret this result as further control of the volcano onto the thrust. Volcanic activity along the strike of the fault is unsteady, and so is, therefore, the subordinate fault. At the western end of the WJBT, the Gede and Salak Volcanoes lie in more southern latitude than the other volcanoes. The shifting of Gede and Salak Volcanoes location could have hindered the westward propagation of the fault.

At the fault scale, the seismic lines also image the interplay with the volcanoes. In many cases, the structure of the fault has several branches, showing that the faulting goes back and forth as the volcano deposits prograde or retrograde. This is well illustrated by the Tampomas (Figure 5a) and Cisanggarung (Figure 6b) Segments, where the progradation of colluvial deposits onto the basin could trigger the transient northward propagation of secondary fault branches. This behavior is also depicted at an even finer scale, on the trench below the Cikamurang ridge: secondary faults initiate, develop and cease their activities in close relation to the sedimentation of the volcanic and volcano-clastic deposits over them (Figure 9).

These results demonstrate the overarching role of volcanoes in the northward propagation of the WJBT. Not only faults are ramping up concurrently to the volcanic activity, but also the volcanic tempo imposes the timing and geometry at scales that range from regional to local. Particularly in West Java, the Quaternary volcanic arc is separated by an intramontane basin south of the Lembang strike-slip fault. The WJBT tectonic model is consistent with the eastern counterpart of the JBT (Lupi et al., 2022), where the magmatic activity spreads upwards through the thrust fault that accompanies the northward propagation of the younger volcanoes. We also compare the WJBT further east with the Flores Back-arc Thrust, where the 2018 Lombok earthquakes attest to the effect of the Rinjani Volcano magmatic system on the dynamics, location, and geometry of the earthquake faults (Lythgoe et al., 2021).

At the scale of Java Island, fault maturity decreases westward from the Kendeng hills in the East Java. In principle, the western end of the WJBT should illustrate the underlying mechanisms that permit this propagation. Yet, while the northward migration of the fault is clear in the eastern side of the WJBT, the westward propagation is less clear. The primordial role that volcanoes exert conversely hides the pattern by imposing an almost discrete change in the fault structure at the longitude of Jatiluhur. Two observations make it difficult to unravel the mechanisms. First, deformation is much younger in the westernmost segments of the faults, underneath the Jakarta Basin, than in the eastern segments. Second, strike-slip gain importance to the west and multiple faults accommodate compression, strike-slip, or a combination of both. While magmatic activity provides a satisfying explanation for the delayed timing of deformation, the reason why partitioning is more developed; west of Jatiluhur remains unclear.

Overall, we can follow the fault trace from east to west, but it gets more complex westward. We take this as evidence of the westward propagation of the WJBT from the well-defined eastern and central segments toward the Bogor Trough and Jakarta Basin. In the west, multiple faults are simultaneously activated until deformation localizes on a more mature fault. Meanwhile, partitioning between strike-slip and shortening prevails over a network of smaller faults. Last, we hypothesize that the greater thickness of the sedimentary cover in those basins may also hamper and delay fault inception at the surface at the western end of the fault system.

We notably identified transpressive faults in the Citarum Segment near Jatiluhur and in the southern part of Jakarta. These observations are in agreement with the regional kinematics of Java, for which both thrust and strike-slip faults have been identified by the structural framework (e.g., Malod, 1995) and by geodetic data (Gunawan & Widiyantoro, 2019; Koulali et al., 2017). Eastward, the strike-slip component gets subtler yet appears in geodetic (Gunawan & Widiyantoro, 2019) and seismicity data (Supendi, Nugraha, Puspito, et al., 2018).

The change of the kinematics between the well-developed compressional regimes in the eastern segments and transpressional regimes in the western segments could be related with the increasing obliquity of the convergence westward (Koulali et al., 2017), and the vicinity of the Sunda strait that articulates the contrasted tectonic frameworks of Java and Sumatra (e.g., Huchon & Le Pichon, 1984). Here, we posit that the interplay with the magmatic activity is also critical and possibly dominant, for fault propagation is hampered by the absence of volcanoes in the westernmost segments. The western segments of the fault show a poor localization of the fault precisely where it is immature. Deformation still occurred until recently, and this has a major influence on fault localization and partitioning of the deformation. If correct, we anticipate that fault segmentation will gradually evolve and that

strike-slip will be offset to the south, in a setting that compares to that of the Cimandiri Fault. Conversely, the northern fault underneath the Jakarta basin will mostly accommodate the convergence, forming a continuous WJBT, across the Jakarta Basin where the currently much less visible thrusts are currently ramping upward.

5.3. Seismological Hazard

We combined several methods to document the geometry of the WJBT and its activity in space and time. We divided it into 12 segments where the WJBT is active. While the eastern segments (Tampomas Segment and Cisanggarung in particular) show the largest bulk deformation, all segments seem to be active at present-day. The deformation includes the western segments in the region of Jakarta and raises the question of the potential hazard that those faults may represent in such a densely populated region, and where infrastructures cluster. A rough approximation of the potential earthquake magnitude for each segment of the WJBT can be made using empirical scaling relationships (e.g., Wells & Coppersmith, 1994). They yield a maximum earthquake magnitude above $6.4 M_w$, for each segment, which is higher than any monitored earthquakes, but could epitomize historical earthquakes such as the 1780 Jakarta earthquake. More recently, a $3.2 M_w$ strike-slip earthquake in 2019 and a $2.4 M_w$ in 2021 (BMKG, repogempa.bmkg.go.id/) struck the Citarum Segment. Likewise, several earthquakes can be assigned to the Ciremai Segment, with magnitudes of $5.5 M_w$ (1990, Ekström et al., 2012), $2.9 M_w$ (2019, BMKG catalog) as well as two shallow earthquake events with thrust fault mechanisms ($3.9 M_w$ and $2.8 M_w$, in 2010 and 2011, Supendi, Nugraha, Puspito, et al., 2018). Further detailed observations of the segments west of Jatiluhur are still needed before a definitive evaluation of the seismic hazard in this region can be made. Eastward, the Cipunegara Segment could have caused a $2.8 M_w$ earthquake event in 2015 (Supendi, Nugraha, Puspito, et al., 2018), and a $3.3 M_w$ in 2021 (BMKG catalog). Of course, it is not surprising that monitored and historical earthquakes belong to these fault segments. However, the tectonic activity that we unraveled on those fault segments reveals that their activity can yield severe hazards that might not be well represented by the relatively low seismic activity that those faults had in the past.

6. Conclusions

Our analysis of the back-arc thrust fault in West Java suggests that the WJBT is a major E-W trending thrust fault system. Its evolution reveals the close interplay with volcanoes, in particular its reliance on the magmatic activity that sets the location, geometry, and timing of each individual faults' activity. WJBT splits into three major regions. Along these three regions, the location of the volcanoes shifts to the south, going westward. In total, we tentatively split the ~ 300 km long WJBT into 12 segments.

Jatiluhur is the pivotal location where the WJBT partitions into structures that are more complex. On the eastern part of Jatiluhur, the WJBT propagates northward. The volcanic arc thrusts the North Java platform. Near the surface, the deformation of the sedimentary layers indicates the development of fault-propagation folds. On the west side of Jatiluhur, bulk deformation is smaller, and folds are occasionally blind. The smaller deformation is evident underneath the Jakarta basin. At the Jakarta basin, the northward progradation is delayed due to the localization of the Salak and Gede Volcanoes that are offset to the south with respect to the strike of the WJBT. In addition, thrusts, strike-slip faults, and transpressive faults structure the basin, while compression prevails East of Jatiluhur.

Our results highlight the Pliocene to recent tectonic activity of the WJBT. The activity in the eastern segments shows that faults deformed Late Pleistocene sediments. In addition, geodetic data and historical earthquakes attest to the sustained activity of the WJBT until the present day. In the western segments, little syn-tectonic sedimentation of the sedimentary layers deposited above the occasionally blind fault and topographic high on the surface attest for an ongoing, recent tectonic activity.

Due to the high seismic hazard of the WJBT, thorough risk evaluation along the WJBT trace is vital to protect the multitude of infrastructure of West Java and its ever-increasing population.

Data Availability Statement

Seismic data were obtained courtesy of Pusdatin ESDM, Indonesia. Seismicity and focal mechanism data are available at <http://repegempa.bmkg.go.id>. DEMs are blended from SRTM30 m and DEMNAS 8-m (<http://tides.big.go.id/DEMNAS>). Figure 1 was done with GMT (Wessel et al., 2019).

Acknowledgments

SA is funded by LPDP scholarship from the Indonesian Government (Grant No. 201808220213319). This study was also supported by National Geographic Society (LH). The authors thank M. M. Mukti, A. Replumaz, L. Audin, M. Chlieh, P. Supendi, and the members of The National Center for Earthquake Studies (Pusgen) for insightful discussions. Nandang, Nyanjang, Sutarman, and Bambang W. Suwargandi are thanked for fieldwork help. We would also like to thank A. Mazzini and an anonymous reviewer for their constructive comments on this article.

References

- Abdurrokhim, & Ito, M. (2013). The role of slump scars in slope channel initiation: A case study from the Miocene Jatiluhur formation in the Bogor Trough, West Java. *Journal of Asian Earth Sciences*, 73, 68–86. <https://doi.org/10.1016/j.jseas.2013.04.005>
- Achdan, A., & Sudana, D. (1992). *Geological map of the Karawang Quadrangles*. Geological Agency of Indonesia. Bandung: Pusat Penelitian dan Pengembangan Geologi.
- Acocella, V., Bellier, O., Sandri, L., Sébrier, M., & Pramumijoyo, S. (2018). Weak Tectono-magmatic relationships along an obliquely convergent plate boundary: Sumatra, Indonesia. *Frontiers of Earth Science*, 6(February), 3. <https://doi.org/10.3389/feart.2018.00003>
- Adamiec, G., & Aitken, M. (1988). Dose rate conversion factors. *Ancient TL*, 29(1), 5–8.
- Aitken, M. J. (1985). Thermoluminescence dating: Past progress and future trends. *Nuclear Tracks and Radiation Measurements*, 10(1–2), 3–6. [https://doi.org/10.1016/0735-245X\(85\)90003-1](https://doi.org/10.1016/0735-245X(85)90003-1)
- Albini, P., Musson, R. M. W., Capera, A. A. G., Locati, M., Rovida, A., Stucchi, M., & Viganò, D. (2013). *Global historical earthquake Archive and catalogue (1000-1903)*. In GEM Technical Report 2013-01 V1.0.0(p. 202).
- Aribowo, S., Muslim, D., Winantris, Natawidjaja, D. H., & Daryono, M. R. (2017). Sub-segmentasi Sesar Pada segmen Kumering Antara Danau Ranau Hingga Lembah Suoh, Lampung Barat. *Jurnal Lingkungan Dan Bencana Geologi*, 692, 31–46.
- Arisbaya, I., Handayani, L., Mukti, M. M., Sudrajat, Y., Grandis, H., & Sumintadireja, P. (2019). Imaging the geometry of Cimandiri Fault zone based on 2D Audio-Magnetotelluric (AMT) model in Nyalindung, Sukabumi–Indonesia. *Pure and Applied Geophysics*, 176, 4833–4845. <https://doi.org/10.1007/s00024-019-02241-0>
- Beckers, J., & Lay, T. (1995). Very broadband seismic analysis of the 1992 Flores, Indonesia, earthquake (Mw = 7.9). *Journal of Geophysical Research*, 100(B9), 18179–18193. <https://doi.org/10.1029/95jb01689>
- Bishop, M. G. (2000). *Petroleum systems of the northwest Java Province, Java and Offshore Southeast Sumatra*. US Department of the Interior, US Geological Survey.
- Castillo, M., Muñoz-Salinas, E., & Ferrari, L. (2014). Response of a landscape to tectonics using channel steepness indices (ksn) and OSL: A case of study from the Jalisco Block, Western Mexico. *Geomorphology*, 221, 204–214. <https://doi.org/10.1016/j.geomorph.2014.06.017>
- Clements, B., Hall, R., Smyth, H. R., & Cottam, M. A. (2009). Thrusting of a volcanic arc: A new structural model for Java. *Petroleum Geoscience*, 15(2), 159–174. <https://doi.org/10.1144/1354-079309-831>
- Darman, H., & Sidi, H. (Eds.). (2000). *An outline of the Geology of Indonesia*. Indonesian Geologists Association publication.
- Daryono, M. R., Natawidjaja, D. H., Sapiie, B., & Cummins, P. (2019). Earthquake Geology of the Lembang Fault, West Java, Indonesia. *Tectonophysics*, 751(July 2018), 180–191. <https://doi.org/10.1016/j.tecto.2018.12.014>
- Daryono, M. R., Rahmawan, M., & Tohari, A. (2016). Surface rupture and geotechnical features of the July 2, 2013 Tanah Gayo earthquake. *Indonesian Journal on Geoscience*, 3(2), 95–105. <https://doi.org/10.17014/ijog.3.2.95-105>
- Djuri, D. (1995). *Geological map of the Arjawinangun Quadrangles*. Geological Agency of Indonesia.
- Durcan, J. A., King, G. E., & Duller, G. A. T. (2015). DRAC: Dose rate and age calculator for trapped charge dating. *Quaternary Geochronology*, 28, 54–61. <https://doi.org/10.1016/j.quageo.2015.03.012>
- Duvall, A., Kirby, E., & Burbank, D. (2004). Tectonic and lithologic controls on bedrock channel profiles and processes in coastal California. *Journal of Geophysical Research*, 109(F3). <https://doi.org/10.1029/2003JF000086>
- Ekström, G., Nettles, M., & Dziewoński, A. M. (2012). The global CMT project 2004–2010: Centroid-moment tensors for 13,017 earthquakes. *Physics of the Earth and Planetary Interiors*, 200–201, 200–201, 1–9. <https://doi.org/10.1016/j.pepi.2012.04.002>
- Flint, J. J. (1974). Stream gradient as a function of order, magnitude, and discharge. *Water Resources Research*, 10(5), 969–973. <https://doi.org/10.1029/WR010i005p00969>
- Galbraith, R. F., & Green, P. F. (1990). Estimating the component ages in a finite mixture. *International Journal of Radiation Applications and Instrumentation - Part D: Nuclear Tracks and Radiation Measurements*, 17(3), 197–206. [https://doi.org/10.1016/1359-0189\(90\)90035-V](https://doi.org/10.1016/1359-0189(90)90035-V)
- Galbraith, R. F., Roberts, R. G., Laslett, G. M., Yoshida, H., & Olley, J. M. (1999). Optical dating of single and multiple grains of quartz from Jinnium rock shelter, northern Australia: Part I, experimental design and statistical models. *Archaeometry*, 41(2), 339–364. <https://doi.org/10.1111/j.1475-4754.1999.tb00987.x>
- Grant Ludwig, L. (2015). 4.21 - Paleoseismology. In G. Schubert (Ed.), *Treatise on Geophysics* (2nd ed., pp. 559–579). Oxford Elsevier. <https://doi.org/10.1016/B978-0-444-53802-4.00088-9>
- Gunawan, E., & Widiyantoro, S. (2019). Active tectonic deformation in Java, Indonesia inferred from a GPS-derived strain rate. *Journal of Geodynamics*, 123(October 2018), 49–54. <https://doi.org/10.1016/j.jog.2019.01.004>
- Hall, R., Clements, B., Smyth, H. R., & Cottam, M. A. (2007). A new interpretation of Java's structure. Indonesian Petroleum Association, Proceedings 31st Annual Convention, pp. 63–86.
- Hall, R., & Smyth, H. R. (2008). *Cenozoic Arc Processes in Indonesia: Identification of the Key Influences on the Stratigraphic Record in Active Volcanic Arcs*. In Formation and applications of the sedimentary record in arc collision zones. *The Geological Society of America Special Paper No 436* (pp. 27–54). [https://doi.org/10.1130/2008.2436\(03\)](https://doi.org/10.1130/2008.2436(03))
- Harris, R., & Major, J. (2017). Waves of destruction in the East Indies: The Wichmann catalogue of earthquakes and tsunami in the Indonesian region from 1538 to 1877. *Geological Society Special Publication*, 441(1), 9–46. <https://doi.org/10.1144/SP441.2>
- Hogg, A. G., Hua, Q., Blackwell, P. G., Niu, M., Buck, C. E., Guilderson, T. P., et al. (2013). SHCal13 Southern Hemisphere calibration, 0–50,000 years cal BP. *Radiocarbon*, 55(04), 1889–1903. https://doi.org/10.2458/azu_js_rc.55.16783
- Huchon, P., & Le Pichon, X. (1984). Sunda strait and central Sumatra fault. *Geology*, 12(11), 668–672. [https://doi.org/10.1130/0091-7613\(1984\)12<668:ssacsf>2.0.co;2.CO;2](https://doi.org/10.1130/0091-7613(1984)12<668:ssacsf>2.0.co;2.CO;2)
- Husson, L., Riel, N., Aribowo, S., Authemayou, C., de Gelder, G., Kaus, B. J. P., et al. (2022). Slow geodynamics and fast morphotectonics in the far East Tethys. *Geochemistry, Geophysics, Geosystems*, 23(1). <https://doi.org/10.1029/2021GC010167>
- Hutchings, S. J., & Mooney, W. D. (2021). The seismicity of Indonesia and tectonic implications. *Geochemistry, Geophysics, Geosystems*, 22(9), 1–42. <https://doi.org/10.1029/2021GC009812>

- Irsyam, M., Cummins, P. R., Asrurifak, M., Faizal, L., Natawidjaja, D. H., Widiyantoro, S., et al. (2020). Development of the 2017 national seismic hazard maps of Indonesia. *Earthquake Spectra*, *36*(1_suppl), 112–136. <https://doi.org/10.1177/8755293020951206>
- Kirby, E., & Whipple, K. X. (2012). Expression of active tectonics in erosional landscapes. *Journal of Structural Geology*, *44*, 54–75. <https://doi.org/10.1016/j.jsg.2012.07.009>
- Kloosterman, F. H. (1989). *Groundwater flow systems in the northern coastal lowlands of West- and Central Java, Indonesia* (Ph.D thesis). Kanisius.
- Koulali, A., McClusky, S., Susilo, S., Leonard, Y., Cummins, P., Tregoning, P., et al. (2017). The kinematics of crustal deformation in Java from GPS observations: Implications for fault slip partitioning. *Earth and Planetary Science Letters*, *458*, 69–79. <https://doi.org/10.1016/j.epsl.2016.10.039>
- Kreutzer, S., Schmidt, C., Fuchs, M., Dietze, M., Fischer, M., & Fuchs, M. (2012). Introducing an R package for luminescence dating analysis. *Ancient TL*, *30*(1), 1–8.
- Leimena, S. L. (1979). Disaster in Bali caused by earthquake 1976 (a Report). *Disasters*, *3*(1), 85–87. <https://doi.org/10.1111/j.1467-7717.1979.tb00203.x>
- Lowick, S. E., Buechi, M. W., Gaar, D., Graf, H. R., & Preusser, F. (2015). Luminescence dating of Middle Pleistocene proglacial deposits from northern Switzerland: Methodological aspects and stratigraphical conclusions. *Boreas*, *44*(3), 459–482. <https://doi.org/10.1111/bor.12114>
- Lupi, M., De Gori, P., Valoroso, L., Baccheschi, P., Minetto, R., & Mazzini, A. (2022). Northward migration of the Javanese volcanic arc along thrust faults. *Earth and Planetary Science Letters*, *577*, 117258. <https://doi.org/10.1016/j.epsl.2021.117258>
- Lythgoe, K., Muzli, M., Bradley, K., Wang, T., Nugraha, A. D., Zulfakriza, Z., et al. (2021). Thermal squeezing of the seismogenic zone controlled rupture of the volcano-rooted Flores Thrust. *Science Advances*, *7*(5), 1–9. <https://doi.org/10.1126/SCIADV.ABE2348>
- Malod, J. A., Karta, K., Beslier, M. O., & Zen, M. T. (1995). From normal to oblique subduction: Tectonic relationships between Java and Sumatra. *Journal of Southeast Asian Earth Sciences*, *12*(1–2), 85–93. [https://doi.org/10.1016/0743-9547\(95\)00023-2](https://doi.org/10.1016/0743-9547(95)00023-2)
- Marliyani, G. I. (2016). *Neotectonics of Java, Indonesia: Crustal Deformation in the Overriding Plate of an Orthogonal Subduction System* (Doctoral thesis). Arizona State University.
- Marliyani, G. I., Arrowsmith, J. R., & Whipple, K. X. (2016). Characterization of slow slip rate faults in humid areas: Cimandiri fault zone, Indonesia. *Journal of Geophysical Research: Earth Surface*, *121*(12), 2287–2308. <https://doi.org/10.1002/2016JF003846>
- Martodjojo, S. (1984). *Evolusi Cekungan Bogor (In Indonesian)* (Doctoral Thesis) Bandung Institute of Technology.
- McCaffrey, R. (1992). Oblique plate convergence, slip vectors, and forearc deformation. *Journal of Geophysical Research*, *97*(B6), 8905–8915. <https://doi.org/10.1029/92JB00483>
- McCaffrey, R. (2009). The tectonic framework of the Sumatran subduction zone. *Annual Review of Earth and Planetary Sciences*, *37*(1), 345–366. <https://doi.org/10.1146/annurev.earth.031208.100212>
- McCaffrey, R., & Nábělek, J. (1987). The geometry of back arc thrusting along the Eastern Sunda Arc, Indonesia: Constraints from earthquake and gravity data. *Journal of Geophysical Research*, *89*(B7), 6171–6179. <https://doi.org/10.1029/jb089ib07p06171>
- Mukti, M. M. (2018). Structural style and depositional history of the Semangko pull apart basin in the southeastern segment of Sumatra fault zone. *RISSET Geologi Dan Pertambangan*, *28*(1), 115–128. <https://doi.org/10.14203/risetgeotam2018.v28.954>
- Natawidjaja, D. H. (2018). Updating active fault maps and sliprates along the Sumatran Fault Zone, Indonesia. *IOP Conference Series: Earth and Environmental Science*, *118*, 12001. <https://doi.org/10.1088/1755-1315/118/1/012001>
- Natawidjaja, D. H., Bradley, K., Daryono, M. R., Aribowo, S., & Herrin, J. (2017). Late quaternary eruption of the Ranau Caldera and new geological slip rates of the Sumatran Fault Zone in southern Sumatra, Indonesia. *Geoscience Letters*, *4*(1). <https://doi.org/10.1186/s40562-017-0087-2>
- Natawidjaja, D. H., Daryono, M. R., Prasetya, G., Udrekliu, P. L. F., & Hananto, N. D. (2021). The 2018 M_w 7.5 Palu “supershear” earthquake ruptures geological fault’s multisegment separated by large bends: Results from integrating field measurements, LiDAR, swath bathymetry and seismic-reflection data. *Geophysical Journal International*, *224*(2), 985–1002. <https://doi.org/10.1093/gji/ggaa498>
- Nguyen, N., Griffin, J., Cipta, A., & Cummins, P. R. (2015). Indonesia’s historical earthquakes. In Modelled examples for improving the national hazard map, Geoscience Australia. <https://doi.org/10.11636/Record.2015.023>
- Pérez-Peña, J. V., Al-Awabdeh, M., Azañón, J. M., Galve, J. P., Booth-Rea, G., & Notti, D. (2017). SwathProfiler and NProfiler: Two new ArcGIS Add-ins for the automatic extraction of swath and normalized river profiles. *Computers & Geosciences*, *104*, 135–150. <https://doi.org/10.1016/j.cageo.2016.08.008>
- Prescott, J. R., & Hutton, J. T. (1994). Cosmic ray contributions to dose rates for luminescence and ESR dating: Large depths and long-term time variations. *Radiation Measurements*, *23*(2), 497–500. [https://doi.org/10.1016/1350-4487\(94\)90086-8](https://doi.org/10.1016/1350-4487(94)90086-8)
- Preusser, F., & Kasper, H. (2001). Comparison of dose rate determination using high-resolution gamma spectrometry and inductively coupled plasma-mass spectrometry. *Ancient TL*, *19*(1), 19–23.
- Puspaningrum, M. R., van den Bergh, G. D., Chivas, A. R., Setiabudi, E., & Kurniawan, I. (2020). Isotopic reconstruction of Proboscidean habitats and diets on Java since the early Pleistocene: Implications for adaptation and extinction. *Quaternary Science Reviews*, *228*, 106007. <https://doi.org/10.1016/j.quascirev.2019.106007>
- Putra, S. D. H., Suryantini, & Srigutomo, W. (2016). Thermal modeling and heat flow density interpretation of the onshore Northwest Java Basin, Indonesia. *Geothermal Energy*, *4*(1), 1–24. <https://doi.org/10.1186/s40517-016-0052-x>
- Ran, W., Luan, X., Lu, Y., Liu, H., Yang, J., Zhao, Y., et al. (2019). Formation and evolution of the tertiary carbonate reefs in the Madura Strait Basin of Indonesia. *Journal of Oceanology and Limnology*, *37*(1), 47–61. <https://doi.org/10.1007/s00343-018-7394-0>
- Ran, W., Luan, X., Lu, Y., Wei, X., Zhang, H., Wang, K., et al. (2020). Seismic characteristics and strontium isotope ages of the Middle Miocene Ngrayong formation in the Madura Strait basin: Implications for the paleogeographic reconstruction of East Java. *Journal of Asian Earth Sciences*, *190*(October), 104109. <https://doi.org/10.1016/j.jseaes.2019.104109>
- Rhodes, E. J. (2011). Optically stimulated luminescence dating of sediments over the past 200,000 years. *Annual Review of Earth and Planetary Sciences*, *39*, 461–488. <https://doi.org/10.1146/annurev-earth-040610-133425>
- Saputra, A., Gomez, C., Delikostidis, I., Zawar-Reza, P., Hadmoko, D. S., Sartohadi, J., & Setiawan, M. A. (2018). Determining earthquake susceptible areas southeast of Yogyakarta, Indonesia—Outcrop analysis from structure from motion (SfM) and geographic information system (GIS). *Geosciences*, *8*(4), 132. <https://doi.org/10.3390/geosciences8040132>
- Sarr, A.-C., Husson, L., Sepulchre, P., Pastier, A.-M., Pedoja, K., Elliot, M., et al. (2019). Subsiding Sundaland. *Geology*, *47*(2), 119–122. <https://doi.org/10.1130/G45629.1>
- Schwanghart, W., & Scherler, D. (2014). Short communication: TopoToolbox 2 - MATLAB-based software for topographic analysis and modeling in Earth surface sciences. *Earth Surface Dynamics*, *2*(1), 1–7. <https://doi.org/10.5194/esurf-2-1-2014>
- Setijadji, L. D., Kajino, S., Imai, A., & Watanabe, K. (2006). Cenozoic island arc magmatism in Java Island (Sunda Arc, Indonesia): Clues on relationships between geodynamics of volcanic centers and ore mineralization. *Resource Geology*, *56*(3), 267–292. <https://doi.org/10.1111/j.1751-3928.2006.tb00284.x>

- Sieh, K., & Natawidjaja, D. (2000). Neotectonics of the Sumatran Fault, Indonesia. *Journal of Geophysical Research*, 105(B12), 28295. <https://doi.org/10.1029/2000JB900120>
- Silver, E. A., Reed, D., & McCaffrey, R. (1983). Back arc thrusting in the E Sunda Arc, Indonesia: A consequence of arc-continent collision. *Journal of Geophysical Research*, 88(B9), 7429–7448. <https://doi.org/10.1029/JB088iB09p07429>
- Simandjuntak, T. O. (1992). Neogene tectonics and orogenesis of Indonesia. *Geological Society of Malaysia*, 33, 43–64. <http://www.gsm.org.my/products/702001-101022-PDF.pdf>
- Simandjuntak, T. O., Barber, A. J. (1996). Contrasting tectonic styles in the neogene orogenic belts of Indonesia. *Geological Society Special Publication*, 106, (106), 185–201. <https://doi.org/10.1144/GSL.SP.1996.106.01.12>
- Smyth, H., Hall, R., Hamilton, J., & Kinny, P. (2005). East Java: Cenozoic basins, volcanoes and ancient basement. *Proceedings of the Indonesian Petroleum Association, 30th Annual Convention* (pp. 251–266). <https://doi.org/10.29118/ipa.629.05.g.045>
- Snyder, N. P., Whipple, K. X., Tucker, G. E., & Merritts, D. J. (2000). Landscape response to tectonic forcing: Digital elevation model analysis of stream profiles in the Mendocino triple junction region, northern California. *GSA Bulletin*, 112(8), 1250–1263. [https://doi.org/10.1130/0016-7606\(2000\)112<1250:LRTTFD>2.0.CO;2](https://doi.org/10.1130/0016-7606(2000)112<1250:LRTTFD>2.0.CO;2)
- Supendi, P., Nugraha, A. D., Puspito, N. T., Widiyantoro, S., & Daryono, D. (2018). Identification of active faults in West Java, Indonesia, based on earthquake hypocenter determination, relocation, and focal mechanism analysis. *Geoscience Letters*, 5(1). <https://doi.org/10.1186/s40562-018-0130-y>
- Supendi, P., Nugraha, A. D., & Widiyantoro, S. (2018). Recent destructive earthquakes around Garut area, West Java, Indonesia: An unidentified fault? *AIP Conference Proceedings*, 1987(July), 1–7. <https://doi.org/10.1063/1.5047362>
- Susilohadi. (1995). Late tertiary and quaternary geology of the east Java basin (Doctor of philosophy thesis, p. 169). University of Wollongong.
- Turkandi, T., Sidarto, D., Agustiyanto, A., & Purbo Hadiwidjoyo, M. M. (1992). *Geological map of Jakarta and Kepulauan Seribu Quadrangles*. Bandung, Indonesia: Geological Agency of Indonesia.
- Valla, P. G., Lowick, S. E., Herman, F., Champagnac, J. D., Steer, P., & Guralnik, B. (2016). Exploring IRSL50 fading variability in bedrock feldspars and implications for OSL thermochronometry. *Quaternary Geochronology*, 36, 55–66. <https://doi.org/10.1016/j.quageo.2016.08.004>
- Van Bemmelen, R. W. (1949). *The Geology of Indonesia, Vol. IA: General Geology of Indonesia and Adjacent Archipelagoes*. Government Printing Office, The Hague. <https://doi.org/10.1080/17512780701768576>
- Walter, T. R., Wang, R., Luehr, B. G., Wassermann, J., Behr, Y., Parolai, S., et al. (2008). The 26 May 2006 magnitude 6.4 Yogyakarta earthquake south of Mt. Merapi volcano: Did lahar deposits amplify ground shaking and thus lead to the disaster? *Geochemistry, Geophysics, Geosystems*, 9(5), 1–9. <https://doi.org/10.1029/2007GC001810>
- Wells, D. L., & Coppersmith, K. J. (1994). New empirical relationships among magnitude, rupture length, rupture width, rupture area, and surface Displacement. *Bulletin of the Seismological Society of America*, 84(4), 974–1002.
- Wessel, P., Luis, J. F., Uieda, L., Scharroo, R., Wobbe, F., Smith, W. H. F., & Tian, D. (2019). The generic mapping tools version 6. *Geochemistry, Geophysics, Geosystems*, 20, 5556–5564. <https://doi.org/10.1029/2019GC008515>
- Wichmann, A. (1918). *The Earthquakes of the Indian Archipelago until the year, 1857(4)*.
- Wobus, C., Whipple, K. X., Kirby, E., Snyder, N., Johnson, J., Spyropolou, K., et al. (2006). Tectonics from topography: Procedures, promise, and pitfalls. *Special Paper of the Geological Society of America*, 398(January), 55–74. [https://doi.org/10.1130/2006.2398\(04\)](https://doi.org/10.1130/2006.2398(04))
- Yang, X., Singh, S. C., & Tripathi, A. (2020). Did the Flores backarc thrust rupture offshore during the 2018 Lombok earthquake sequence in Indonesia? *Geophysical Journal International*, 221(2), 758–768. <https://doi.org/10.1093/gji/ggaa018>
- Yeh, H., Imamura, F., Synolakis, C., Tsuji, Y., Liu, P., & Shi, S. (1993). The Flores island tsunamis. *Eos, Transactions American Geophysical Union*, 74(33), 369–373. <https://doi.org/10.1029/93EO00381>
- Zahirovic, S., Matthews, K. J., Flament, N., Müller, R. D., Hill, K. C., Seton, M., & Gurnis, M. (2016). Tectonic evolution and deep mantle structure of the eastern Tethys since the latest Jurassic. *Earth-Science Reviews*, 162, 293–337. <https://doi.org/10.1016/j.earscirev.2016.09.005>